Composite Structures 172 (2017) 173–189

Contents lists available at ScienceDirect

Composite Structures

journal homepage: www.elsevier.com/locate/compstruct

Free vibration and buckling of foam-filled composite corrugated sandwich plates under thermal loading

Bin Han [a,b,*], Ke-Ke Qin [b,c], Qian-Cheng Zhang [b,c], Qi Zhang [a], Tian Jian Lu [b,c,*], Bing-Heng Lu [a]

[a] School of Mechanical Engineering, Xi'an Jiaotong University, Xi'an 710049, China
[b] MOE Key Laboratory for Multifunctional Materials and Structures, Xi'an Jiaotong University, Xi'an 710049, China
[c] State Key Laboratory for Mechanical Structure Strength and Vibration, Xi'an Jiaotong University, Xi'an 710049, China

ARTICLE INFO

Article history:
Received 26 May 2016
Revised 20 January 2017
Accepted 14 March 2017
Available online 28 March 2017

Keywords:
Composite sandwich plate
Foam-filled corrugated core
Refined shear theory
Thermal loading

ABSTRACT

The free vibration and buckling behaviors of foam-filled composite corrugated sandwich plates under thermal loading are investigated theoretically. A refined shear deformation theory is extended incorporating two different combinations of hyperbolic and parabolic shear shape functions. Equivalent thermoelastic properties of the foam-filled corrugation are obtained using the method of homogenization based on the Gibbs free energy. Based on hyperbolic-polynomial variation of all displacements across the thickness of both face sheets and sandwich core, the shear plate theory accounts for both transverse shear and thickness stretching effects. The theoretical predictions are validated against existing results as well as finite element simulations. The effects of geometric and material parameters on natural frequency and critical temperature change for buckling are systematically investigated. The proposed theory is not only accurate but also simple in predicting the free vibration and thermal buckling responses of composite sandwich plates with foam-filled corrugated cores.

1. Introduction

Sandwich plates with periodic lattice cores such as pyramidal trusses and square honeycombs possess superior bending stiffness, strength and shock resistance with respect to monolithic plates of the same mass, and present opportunities for additional functionality, such as vibration control, thermal transport and energy absorption [1,2]. As one type of lattice topologies, two-dimensional (2D) corrugated panels as sandwich core have enjoyed widespread applications in areas of packaging, building and transportation industry (e.g., skin frame of high-speed train, naval craft and rocket engine shell), which is attributed mainly to their relatively low cost, ease of fabrication and reparability, flexibility in design, and good structural performance [3]. However, under compressive loading, a corrugated sandwich core first deforms by stretching of its struts (core webs) and then collapses by Euler or plastic buckling at a small strain, softening rapidly due to node failure and/or core buckling. Metallic corrugations are thus less attractive for energy absorption applications as large forces are transferred but limited amount of energy is absorbed [4]. Moreover, the transverse shear and bending resistance of corrugated sandwiches are somewhat limited, since corrugated panels are prone to buckle under such loading conditions [5,6].

Recently, in order to enhance the mechanical properties (*e.g.*, specific strength and specific energy absorption) of corrugated sandwich cores, the concept of filling foam into the interstice of corrugations has been exploited, both experimentally and theoretically [7–15]. These studies demonstrated that the performance benefits of foam filling derive mainly from the stabilizing effects of foam on the buckling and post-buckling of the corrugated panels (and face sheets). The foam-filled corrugated sandwich structures have applied as the explosion-proof plates of armored vehicles and shell of oil tanks due to their great mechanical performance and good fire resistance [16]. However, there is yet a study concerning free vibration and stability of a sandwich plate having foam-filled corrugated core, either its face sheets and core members are made of metal or fiber-reinforced composite. The applicability of such sandwich structures could also extend to be used in the severe thermal environments such as radomes, cryotanks, high speed spacecraft, and nuclear reactors, etc, where the thermal environment is a key factor which changes the stiffness of the structural system and alters the dynamic characteristics of the system essentially. Therefore, it is of great importance to make an intensive research on the vibration and stability characters of such sandwich structures (especially made of composite materials) in high temperature environment.

* Corresponding authors at: School of Mechanical Engineering, Xi'an Jiaotong University, Xi'an 710049, China (B. Han). MOE Key Laboratory for Multifunctional Materials and Structures, Xi'an Jiaotong University, Xi'an 710049, China (T.J. Lu).

E-mail addresses: hanbinghost@mail.xjtu.edu.cn (B. Han), tjlu@mail.xjtu.edu.cn (T.J. Lu).

http://dx.doi.org/10.1016/j.compstruct.2017.03.051
0263-8223/

Nomenclature

ρ_s	density of the face sheets or corrugated panels
ρ_f	density of foam
ρ_c	density of foam-filled corrugated sandwich core
λ	volume fraction of the corrugated panels in the core
t	corrugated member thickness
l	corrugated member length
θ	corrugation angle
a	plate length
b	plate width
h	total thickness
h_f	face sheet thickness
h_c	core height
E_i, G_{ij}, υ_{ij}	elastic modulus, shear modulus, and Poisson's ratio
α_i	thermal expansion coefficient
$x-y-z$	global coordinate system of sandwich plates
$\bar{x}-\bar{y}-\bar{z}$	local coordinate system of the unit cell of foam-filled corrugated core
$x_1-x_2-x_3$	local coordinate system of corrugated panel,
$y_1-y_2-y_3$	material coordinate systems of face sheets
C_{ij}^H	material coordinate systems of corrugated panels
β_i^H	effective stiffness of foam-filled corrugated core
c^H	effective thermal-stress tensor of foam-filled corrugated core
β_i^H	effective specific heat per unit volume of the unit cell of foam-filled corrugated core
u, v, w	generalized displacement field functions
u_0, V_0, w_b, w_s, φ_z	unknown functions of the refined shear deformation theory
$f(z)$, $g(z)$	shape function
σ_x^0, σ_y^0, τ_{xy}^0	initial in-plane thermal stresses
ΔT	temperature variation
ΔT_{cr}	critical buckling temperature change
ω	natural frequency
$\bar{\omega}, \overline{\Delta T_{cr}}$	dimensionless natural frequency and critical buckling temperature change
$[\mathbf{K}]$	structural stiffness matrix
$[\mathbf{K}_G]$	geometric stiffness matrix induced by initial in-plane thermal stresses
$[\mathbf{M}]$	mass matrix

There are several literatures carried out on lattice-cored sandwich plates or beams to reveal the global structural analysis (*e.g.*, vibration and buckling), with the discrete lattice core usually treated as an equivalent homogenous transverse isotropic or orthotropic continuum [17–19]. However, few studies have been done in the field of vibration and stability behaviors for the lattice-cored sandwich structures under thermal environment. All the studies about the lattice sandwiches employed the simple first-order shear deformation theory (FSDT). This theory assumes that the face sheets deform according to the Bernoulli-Euler beam theory or Kirchhoff-Love plate theory, the core deforms only in shear with transverse shear stress assumed constant through the thickness of the core, and the effect of thickness stretching (*i.e.*, transverse normal strains) is negligible. FSDT is only efficient for sandwich plates with thin hard face sheets and thick soft core. For sandwich plates with thick multi-layered laminated composite face sheets and relatively hard core, the above assumptions may not hold. Since FSDT does not satisfy the stress-free surface conditions, and only accounts for layerwise constant states of transverse shear stress, shear correction coefficients are usually needed to rectify the unrealistic variation of shear strain/stress through thickness, which ultimately defines the shear strain energy. To address this issue, several higher-order shear deformation theories (HSDTs), *e.g.*, polynomial, trigonometric, exponential and hyperbolic shear deformation theories, have been developed as the Equivalent Single Layer (ESL) theories, LayerWise (LW) theories, and the Zigzag (ZZ) theories, as shown in recent reviews of laminated composites and sandwich plates [20–22] and functionally graded materials (FGMs) [23–26]. Reddy [27] developed a well-known third order shear deformation theory which is further extended by many researchers for their research. The trigonometric shear deformation theories were proposed for the free vibration of thick orthotropic plates by Touratier [28] and Mantari et al. [29], etc. Karama et al. [30] proposed an exponential variation for the transverse strain in their investigation of the bending of composite beams, which is developed by Aydogdu [31] for the analysis of laminated composite plates. Soldatos [32] has developed hyperbolic shear deformation theory for the analysis of laminated composite and sandwich plates, which was applied by Ghugal and Pawar [33] for the free vibration analysis of orthotropic plates. Zenkour [34] and Amale et al. [35] have employed separately hyperbolic sine and hyperbolic tangent shear deformation theories for the bending and free vibration analysis of FG plates. Recently, Grover et al. [36] developed inverse hyperbolic shear deformation theory for the free vibration analysis of laminated composite and sandwich plates using finite element modelling.

Aydogdu [37] compared a group of shear deformation theories for analyzing the bending, buckling, and vibration behaviors of rectangular symmetric cross-ply plates with simply supported edges. The results revealed that while the transverse displacement and stresses are best predicted by the exponential shear deformation theory, the parabolic shear deformation and hyperbolic shear deformation theories yield more accurate predictions of the natural frequency and buckling load. To reduce the number of variables in existing theories, a kind of refined shear deformation theory (RST) as ESL theories, incorporating various higher-order shear deformation formulations, has been developed [38–44]. RST assumes that the in-plane and transverse displacements contain bending and shear components, with strong similarities with FSDT in many aspects such as equations of motion, boundary conditions, and stress resultant expressions. At present, RST has been mostly applied to FGM plates, but barely to sandwich or laminated plates.

The aim of the paper is focused on extending the original RST formulation to vibration and buckling problems of foam-filled composite corrugated sandwich plates under uniform thermal loading. The refined shear and normal deformation theory is employed and two different combinations of hyperbolic and parabolic shear shape functions are adopted. The sandwich core is taken as an equivalent homogenous continuum layer so that the sandwich itself could be regarded as an orthotropic multi-layered plate. All the effective thermoelastic material parameters of the foam-filled composite corrugated core are then derived via the homogenization method for the first time. Different from previous researches about the vibration of lattice-cored sandwich plates, the bending, transverse shear, and thickness stretching of both the face sheets and the core are all taken into account. Governing equations are derived using the Hamilton principle and solutions for simply-supported sandwich plates are obtained using the Navier's technique. The validity of the proposed theory is demonstrated through comparison with the results from literature and finite element (FE) simulations. The effects of thickness stretching, geometric parameters and foam filling material on critical temperature change and natural frequency are systematically explored.

2. Mathematical formulation

With reference to Fig. 1, consider a sandwich plate comprising two fiber-reinforced composite cross-ply laminates of equal thickness as face sheets and a foam-filled corrugated core. Relevant geometric variables are: sandwich plate length a, width b, and total thickness h; face sheet thickness h_f; core height h_c; corrugated member thickness t, length l, and corrugation angle θ.

The hybrid sandwich core is assumed to be constructed of linearly elastic isotropic foam fillers and corrugated panels made of orthotropic unidirectional laminate. Macroscopically, the hybrid core may be treated as a homogeneous equivalent core with orthotropic material properties, as depicted in Fig. 2. Let E_i, ν_{ij} and α_i (i, j = 1, 2, 3) denote the elastic modulus, Poisson ratio and thermal expansion coefficient of the laminated composite making either face sheets or corrugated panels. Let E_f, ν_f and α^f denote the elastic modulus, Poisson ratio and thermal expansion coefficient of the foam. Let ρ_s and ρ_f represent the density of the face sheets and the foam. The volume fraction λ of the corrugated panels ($\lambda = 2t/l\sin 2\theta$) and the density ρ_c of the hybrid sandwich core can be obtained using the method detailed by Han et al. [14].

For foam filling, both polymer foam (Rohacell) and aluminum foam (Alporas) are considered. In addition to carbon fiber-reinforced composite material (T700/3234), face sheets and corrugated members made of 304 stainless steel or titanium alloy (Ti-6Al-4V) are also considered.

The assumptions made for the present study are:

(1) The behavior of the sandwich falls within the state of small deformation and linear elasticity.
(2) The face sheets and corrugated panels are made of the same parent material.
(3) Local responses such as localized vibration or buckling are not considered.
(4) No slippage or delamination between composite layers occurs.
(5) The material properties are temperature-independent.
(6) The sandwich is placed in high temperature environment sufficiently long, so that its temperature is distributed uniformly and uniform temperature rise is in force.
(7) The corrugated core members and the filling foam keep close contact with each other during deformation, even though slipping may occur at the interface.

2.1. Effective thermoelastic properties of foam-filled composite corrugation

To analyze the free vibration and stability of the composite sandwich plate of Fig. 1 under thermal loading, the effective thermoelastic properties of its foam-filled composite corrugated core are firstly derived by employing the method of energy-based thermomechanical homogenization [45]. The foam-filled corrugated core may be analyzed at two different scales: (a) at the macroscale, it is treated as a homogeneous continuum solid; (b) at the microscale, the foam fillers and the corrugated members are separately considered. The derivation of micro-macro relations for such a periodic medium relies on the analysis of its representative volume element (RVE, or unit cell; Fig. 2), as detailed below.

When subjected to a $\bar{x}-\bar{z}$ plane macroscopic strain $\mathbf{E}$ (Fig. 3a), the corrugated member may be characterized as an Euler-Bernoulli beam of unit width (along the $\bar{y}$-direction), clamped at both ends [14], where the Cartesian coordinate system $\bar{x}-\bar{y}-\bar{z}$ is set based upon the unit cell of foam-filled corrugated sandwich core. Analogous to the analysis of a pin-reinforced foam core [46], the macroscopic Gibbs free energy density of the unit cell containing two corrugated beam members surrounded by foam filling (Fig. 2) may be written as:

$$G = G_b + G_f \tag{1}$$

$$G_b = \frac{1}{\Omega}\sum_{i=1}^{2}\left[\frac{1}{2}\left(\tilde{\mathbf{u}}^{(i)} + 2\tilde{\mathbf{u}}_p^{(i)} - 2\tilde{\mathbf{u}}_{\Delta T}^{(i)}\right)^T \tilde{\mathbf{K}}^{(i)}\tilde{\mathbf{u}}^{(i)} - \frac{1}{2}\frac{c^{(i)}\Delta T^2}{T_0}V^{(i)} - \tilde{g}_p^{(i)}\right] \tag{2}$$

$$G_f = (1-\lambda)\left(\frac{1}{2}C^f_{hjkl}E_{hj}E_{kl} - \Delta T C^f_{hjkl}\alpha^f_{hj}E_{kl} - \frac{1}{2}\frac{c^f}{T_0}\Delta T^2\right) + \frac{1}{\Omega}\sum_{i=1}^{2}\tilde{g}_p^{(i)} \tag{3}$$

where G_b and G_f are the free-energy contributions of corrugated members and foam, respectively, Ω represents the current volume of the unit cell, superscript/subscript f denotes the foam filler, c is

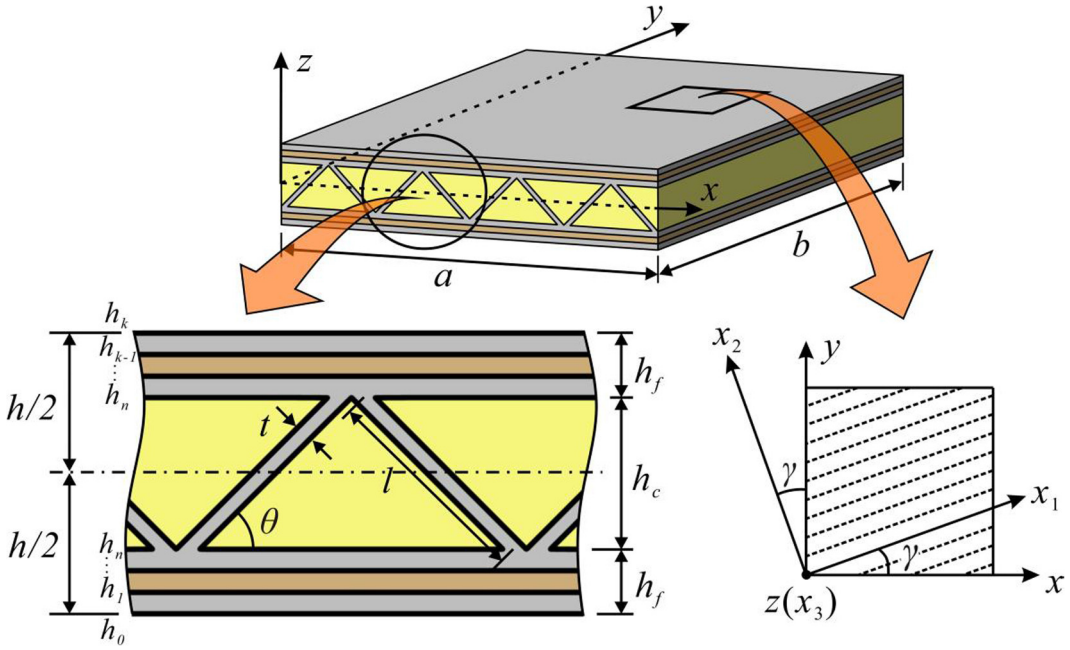

Fig. 1. Schematic of foam-filled composite corrugated sandwich plate with cross-ply laminated face sheets ($\gamma = 0^\circ, 90^\circ$).

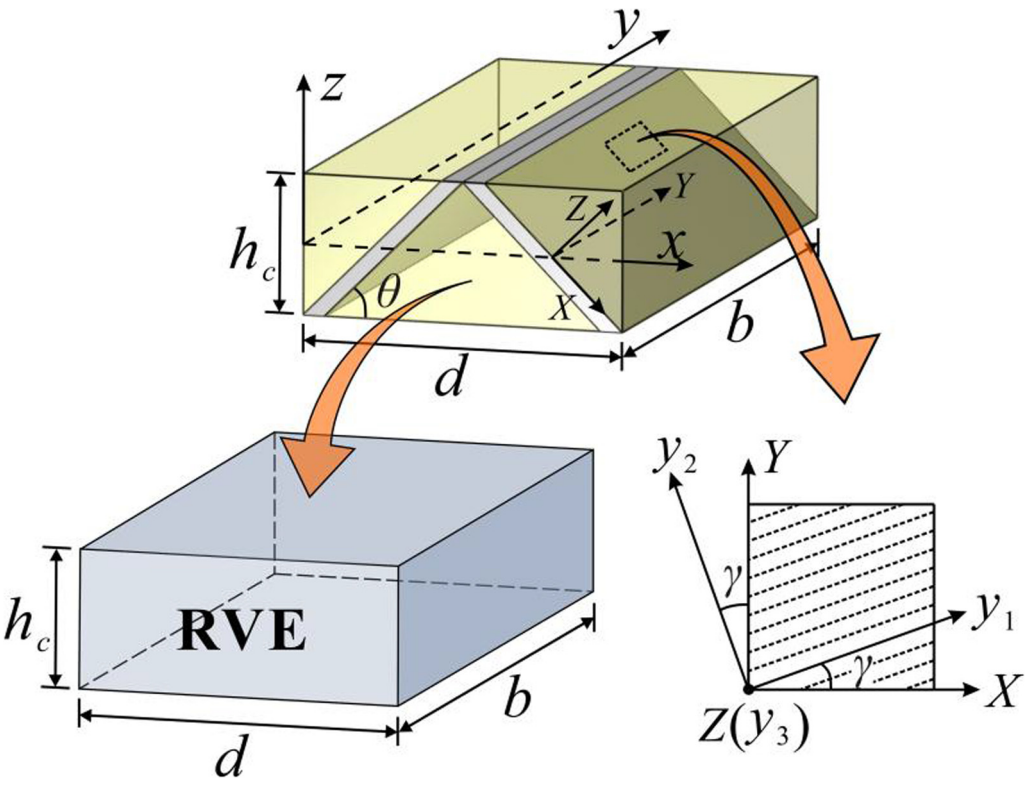

Fig. 2. Representative volume element (RVE) of foam-filled corrugated core, with corrugated panels made of unidirectional laminate composite ($\gamma = 0^\circ, or 90^\circ$).

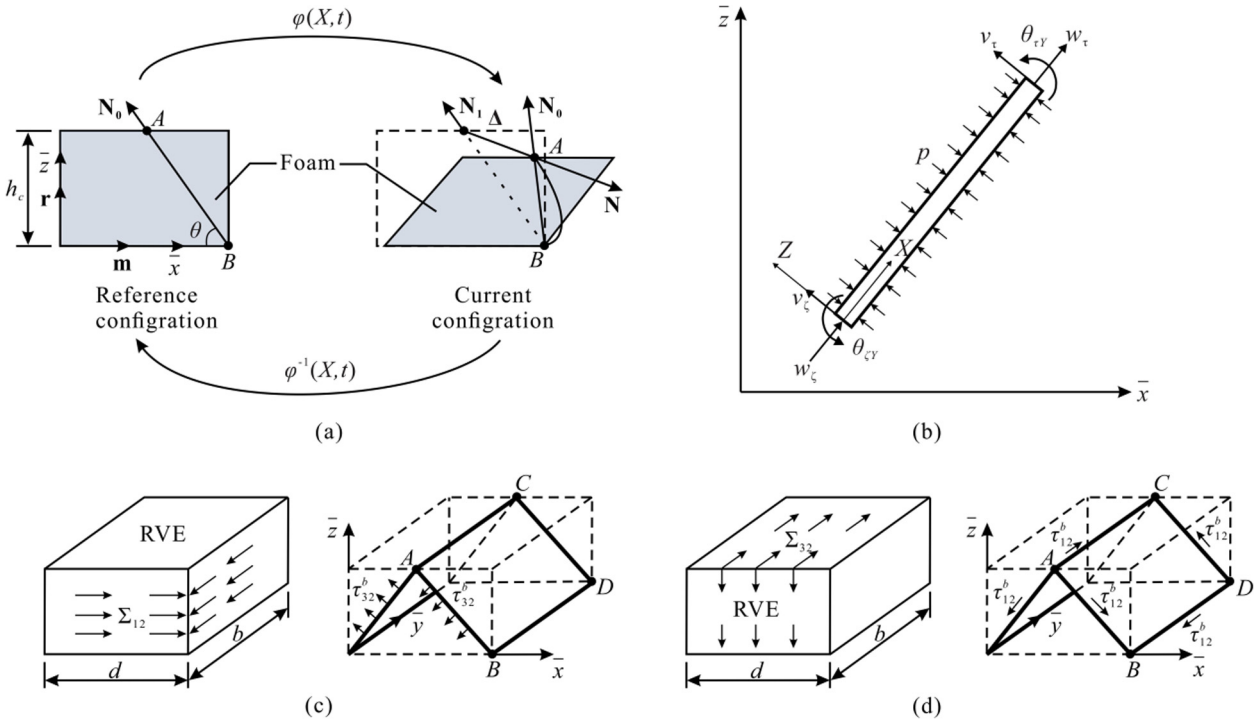

Fig. 3. Homogenization of foam-filled corrugation in plane strain: (a) kinematics of a corrugated member; (b) a corrugated member subjected to nodal forces/moments and lateral pressure. Shear flow in a typical representative volume element when subjected to (c) macroscopic shear strain E_{12} or (d) macroscopic shear strain E_{23}.

the specific heat per volume at constant strain, C^f_{hjkl} is the elastic constant of foam, E_{hj} is the macroscopic strain, $V^{(i)}$ denotes the volume of the ith corrugated member, and T_0 represents the initial temperature of the field. $\tilde{\mathbf{u}}^{(i)}$ is the global nodal displacement vector for the i-th inclined beam characterized by end nodes, of which a detailed description can be found in [14]. $\tilde{\mathbf{u}}^{(i)}_p$ and $\tilde{\mathbf{u}}^{(i)}_{\Delta T}$ are the nodal displacement vectors of the ith beam induced by lateral normal stress $p^{(i)}$ (Fig. 3b) and temperature variation ΔT:

$$\tilde{\mathbf{u}}_p^{(i)} = \mathbf{T}^T \tilde{\mathbf{u}}_p^{(i)e}, \quad \tilde{\mathbf{u}}_{\Delta T}^{(i)} = \mathbf{T}^T \tilde{\mathbf{u}}_{\Delta T}^{(i)e} \tag{4}$$

$$\tilde{\mathbf{u}}_p^{(i)e} = \left[\frac{\nu_{31} p^{(i)}}{E_3/(1-\nu_{13}\nu_{31})} l \quad 0 \quad 0 \quad 0 \quad 0 \quad 0\right]^T \tag{5}$$

$$\tilde{\mathbf{u}}_{\Delta T}^{(i)e} = [\alpha_1 \Delta T l \quad 0 \quad 0 \quad 0 \quad 0 \quad 0]^T \tag{6}$$

where $\mathbf{T}$ is the transformation matrix between local and global coordinates and the superscript e denotes values in local coordinates. Note that, representing the coupling effect between corrugated beam and foam, the lateral normal stress $p^{(i)}$ is itself induced by the foam matrix, of which the detailed expression can be found in Han et al. [14].

In Eq. (2), $\tilde{\mathbf{K}}^{(i)}$ is the global stiffness matrix that satisfies the transformation between local and global coordinates, as:

$$\tilde{\mathbf{K}}^{(i)} = \mathbf{T}^T \mathbf{K}^{e(i)} \mathrm{T} \tag{7}$$

where $\mathrm{K}^{e(i)}$ is the elementary stiffness matrix of the ith beam, of which a detailed expression is presented in [14], with the elastic modulus E_s replaced by $E_1/(1-\nu_{13}\nu_{31})$.

Let the macroscopic strain vector of the unit cell be defined as:

$$\begin{aligned}\boldsymbol{\Xi} &= [\Xi_1 \quad \Xi_2 \quad \Xi_3 \quad \Xi_4 \quad \Xi_5 \quad \Xi_6]^T \\ &= [E_{11} \quad E_{22} \quad E_{33} \quad 2E_{12} \quad 2E_{13} \quad 2E_{23}]^T\end{aligned} \tag{8}$$

Then the effective stiffness $\mathbf{C}^H$, the effective thermal-stress tensor $\boldsymbol{\beta}^H$ and the effective specific heat per unit volume of the unit cell c^H can be calculated as:

$$C_{ij}^H = \frac{\partial^2 G}{\partial \Xi_i \partial \Xi_j}, \quad \beta_i^H = -\frac{\partial^2 G}{\partial \Delta T \partial \Xi_i}, \quad c^H = -\frac{\partial^2 G}{\partial \Delta T \partial \Delta T} \tag{9}$$

where the superscript H means homogenized effective stiffness. The $\bar{x}-\bar{z}$ plane macroscopic effective stiffness and thermal-stress tensor for a foam-filled corrugated core may thence be obtained using Eq. (9), as:

$$\begin{aligned}
C_{11}^H &= \frac{E_1}{(1-\nu_{13}\nu_{31})}\left(\frac{t}{l}\right)\frac{\cos^3\theta}{\sin\theta} + \frac{E_1}{(1-\nu_{13}\nu_{31})}\left(\frac{t}{l}\right)^3 \sin\theta\cos\theta \\
&\quad + 2\nu_{13}\left(\frac{t}{l}\right)(\sin^2\theta C_{11}^f + \cos^2\theta C_{13}^f)\frac{\cos\theta}{\sin\theta} + (1-\lambda)C_{11}^f \\
C_{33}^H &= \frac{E_1}{(1-\nu_{13}\nu_{31})}\left(\frac{t}{l}\right)\frac{\sin^3\theta}{\cos\theta} + \frac{E_1}{(1-\nu_{13}\nu_{31})}\left(\frac{t}{l}\right)^3 \sin\theta\cos\theta \\
&\quad + 2\nu_{13}\left(\frac{t}{l}\right)(\sin^2\theta C_{13}^f + \cos^2\theta C_{33}^f)\frac{\sin\theta}{\cos\theta} + (1-\lambda)C_{33}^f \\
C_{13}^H &= \frac{E_1}{(1-\nu_{13}\nu_{31})}\left(\frac{t}{l}\right)\sin\theta\cos\theta - \frac{E_1}{(1-\nu_{13}\nu_{31})}\left(\frac{t}{l}\right)^3 \sin\theta\cos\theta \\
&\quad + \nu_{13}\left(\frac{t}{l}\right)\left[\frac{\sin^3\theta}{\cos\theta}C_{11}^f + \sin 2\theta C_{13}^f + \frac{\cos^3\theta}{\sin\theta}C_{33}^f\right] + (1-\lambda)C_{13}^f \\
C_{55}^H &= \frac{E_1}{(1-\nu_{13}\nu_{31})}\left(\frac{t}{l}\right)\sin\theta\cos\theta + \frac{E_1}{(1-\nu_{13}\nu_{31})}\left(\frac{t}{l}\right)^3 \\
&\quad \times \frac{(\cos^2\theta - \sin^2\theta)^2}{4\sin\theta\cos\theta} - 4\nu_{13}\left(\frac{t}{l}\right)C_{55}^f \sin\theta\cos\theta + (1-\lambda)C_{55}^f \\
\beta_1^H &= \frac{E_1}{(1-\nu_{13}\nu_{31})}\left(\frac{t}{l}\right)\alpha_1\frac{\cos\theta}{\sin\theta} + (1-\lambda)(C_{11}^f + 2C_{13}^f)\alpha^f \\
\beta_3^H &= \frac{E_1}{(1-\nu_{13}\nu_{31})}\left(\frac{t}{l}\right)\alpha_1\frac{\sin\theta}{\cos\theta} + (1-\lambda)(C_{33}^f + 2C_{13}^f)\alpha^f \\
C_{15}^H &= C_{35}^H = \beta_5^H = 0
\end{aligned} \tag{10}$$

If a macroscopic strain E_{22} is solely imposed on the core, the stress of core member σ_y^b (with foam-corrugation coupling included) and the stress of foam matrix σ_y^f are given by:

$$\sigma_y^b = \frac{E_2}{(1-\nu_{12}\nu_{21})}(E_{22} - \alpha_2\Delta T) + \nu_{23}(\sin^2\theta C_{12}^f + \cos^2\theta C_{23}^f)E_{22} \tag{11}$$

$$\sigma_y^f = C_{22}^f(E_{22} - \alpha^f \Delta T) \tag{12}$$

It follows that the macroscopic stress is:

$$\sigma_y = \lambda\sigma_y^b + (1-\lambda)\sigma_y^f \tag{13}$$

so that

$$\begin{aligned}
C_{22}^H &= \lambda\left[\frac{E_2}{(1-\nu_{12}\nu_{21})} + \nu_{23}\left(\sin^2\theta C_{12}^f + \cos^2\theta C_{23}^f\right)\right] + (1-\lambda)C_{22}^f \\
\beta_2^H &= \frac{\lambda\alpha_2 E_2}{(1-\nu_{12}\nu_{21})} + (1-\lambda)\alpha^f C_{22}^f
\end{aligned} \tag{14}$$

When E_{11} or E_{33} is solely imposed on the unit cell, σ_y can be solved using nodal displacements and the corresponding equilibrium equations, with coupling effect included. Consequently, C_{12}^H and C_{23}^H can be obtained as:

$$\begin{aligned}
C_{12}^H &= \frac{\nu_{12}E_2}{(1-\nu_{12}\nu_{21})}\left(\frac{t}{l}\right)\frac{\cos\theta}{\sin\theta} + \nu_{23}\left(\frac{t}{l}\right)\frac{\sin^2\theta C_{11}^f + \cos^2\theta C_{13}^f}{\sin\theta\cos\theta} + (1-\lambda)C_{12}^f \\
C_{23}^H &= \frac{\nu_{12}E_2}{(1-\nu_{12}\nu_{21})}\left(\frac{t}{l}\right)\frac{\sin\theta}{\cos\theta} + \nu_{23}\left(\frac{t}{l}\right)\frac{\sin^2\theta C_{13}^f + \cos^2\theta C_{33}^f}{\sin\theta\cos\theta} + (1-\lambda)C_{23}^f
\end{aligned} \tag{15}$$

When subjected to macroscopic shear strain E_{12} or E_{23}, the resulting distributed shear flow in the unit cell is presented in Fig. 3c and d, respectively, in which cases the foam-corrugation coupling effect vanishes. The macroscopic shear stress Σ_{1i} can be expressed as

$$\Sigma_{2i} = \Sigma_{2i}^b + \Sigma_{2i}^f, \quad (i = 1, 3) \tag{16}$$

where Σ_{2i}^b and Σ_{2i}^f represent the contributions from corrugated member and foam, respectively. Further, we have

$$\begin{aligned}
&\Sigma_{12}^b\Omega = 2\tau_{23}^b tl\sin\theta, \quad \Sigma_{23}^b\Omega = 2\tau_{12}^b tl\sin\theta, \\
&\Sigma_{12}^f = (1-\lambda)C_{44}^f E_{12}, \quad \Sigma_{23}^f = (1-\lambda)C_{66}^f E_{23}
\end{aligned} \tag{17}$$

where τ_{23}^b and τ_{12}^b are the shear stresses of corrugated member in local ordinate system X-Y-Z. For both shear loading cases (E_{12} and E_{23}), due to the symmetric layout of the unit cell, all the inclined core members bear the same local out-of-plane shear stresses. The local shear strains can be written accordingly, as:

$$\varepsilon_{12} = \frac{\tau_{23}^b}{2G_{23}}, \quad \varepsilon_{23} = \frac{\tau_{12}^b}{2G_{12}} \tag{18}$$

Energy balance of the corrugated members dictates thence that:

$$\begin{aligned}
&\tfrac{1}{2}C_{44}^{Hb}(2E_{12})^2\Omega = \tfrac{1}{2}G_{23}\left(\tfrac{\tau_{23}^b}{G_{23}}\right)^2 tl \\
&\tfrac{1}{2}C_{66}^{Hb}(2E_{23})^2\Omega = \tfrac{1}{2}G_{12}\left(\tfrac{\tau_{12}^b}{G_{12}}\right)^2 tl
\end{aligned} \tag{19}$$

from which:

$$C_{44}^{Hb} = G_{23}\left(\frac{t}{l}\right)\frac{\sin\theta}{\cos\theta}, \quad C_{66}^{Hb} = G_{12}\left(\frac{t}{l}\right)\frac{\sin\theta}{\cos\theta} \tag{20}$$

Consequently, we have:

$$C_{ii}^H = C_{ii}^{Hb} + (1-\lambda)C_{ii}^f \quad (i = 4, 6) \tag{21}$$

Since a corrugated core is orthotropic, the remaining components of the macroscopic stiffness matrix and thermal-stress tensor are all zeroes. Finally, the vector of effective thermal expansion coefficients, $\boldsymbol{\alpha}^H$, can be finally obtained as

$$\boldsymbol{\alpha}^H = \left[\mathbf{C}^H\right]^{-1}\boldsymbol{\beta}^H \tag{22}$$

2.2. Generalized displacement field and kinematic relationship

The refined plate theories developed recently have only five unknown functions [40,44,47–49], in which the in-plane displacements are expanded as odd functions of the thickness coordinate while the transverse displacement is splitted into bending, shear and thickness stretching parts, as:

$$\begin{cases} u(x,y,z) = u_0(x,y) - z\frac{\partial w_b}{\partial x} - f(z)\frac{\partial w_s}{\partial x} \\ v(x,y,z) = v_0(x,y) - z\frac{\partial w_b}{\partial y} - f(z)\frac{\partial w_s}{\partial y} \\ w(x,y,z) = w_b(x,y) + w_s(x,y) + g(z)\varphi_z(x,y) \end{cases} \tag{23}$$

where $u_0(x,y)$, $v_0(x,y)$, $w_b(x,y)$, $w_s(x,y)$, and $\varphi_z(x,y)$ are the five unknown functions of the plate (which is defined in the global Cartesian coordinate system $x-y-z$, as shown in Fig. 1), and $f(z)$ is the shape functions determining the distribution of transverse shear strains and stresses along the thickness:

$$f(z) = z - \chi z - \phi(z) \tag{24}$$

The function $\phi(z)$ and the prescribed parameter χ are listed in Table 1. The function g(z) in (23) is defined as:

$$g(z) = 1 - f'(z) = \chi + \phi'(z) \tag{25}$$

As a compact formulation, the above displacement field can take into account different displacement-based shear deformation functions. Upon taking $\phi(z) = 0$ and χ as either 0 or 1, the classical plate theory (CPT) or simple first-order shear deformation theory (SFSDT) [50] can be obtained as particular cases, as shown in Table 1. In addition to CPT and FSDT, the stress free boundaries at the top and bottom surfaces of the sandwich plate can be satisfied automatically by employing higher-order shear shape functions (such as polynomial (PSDT) [27,51,52], sinusoidal (SSDT) [28], tangential (TSDT) [29], hyperbolic-sin (HSSDT) [33], hyperbolic-tangent (HTSDT) [53], exponential (ESDT) [30], combined sinusoidal and exponential (SESDT) [54], and combined hyperbolic-sin and exponential ones (HSESDT) [44], as summarized in Table 1), without requiring any shear correction factor. With these higher-order shear deformation theories, the cases without including the effect of thickness stretching can be considered when $\varphi_z(x,y)$ vanishes. In the present study, two different shape functions, i.e. the combined hyperbolic sinusoidal and polynomial shear deformation theory (HSPSDT) [34] and the combined hyperbolic tangent and polynomial shear deformation theory (HTPSDT) [35], are selected for the refined shear deformation theories (RSTs), as shown in Table 1.

Table 1
Shape functions employed by different plate theories for generalized displacement field.

Models	Shape functions	
	$\phi(z)$	χ
CPT	0	0
SFSDT [50]	0	1
PSDT1 [51]	$-\frac{z^3}{6}$	$\frac{h^2}{8}$
PSDT2 [52]	$-\frac{5}{3}z\left(\frac{z}{h}\right)^2$	$\frac{5}{4}$
PSDT3 [27]	$-\frac{4}{3}\frac{z^3}{h^2}$	1
SSDT [28]	$\frac{h}{\pi}\sin\left(\frac{\pi z}{h}\right)$	0
TSDT [29]	$\tan\left(\frac{z}{5h}\right)$	$-\frac{1}{5h}\sec^2\left(\frac{1}{10}\right)$
HSSDT [32]	$h\sinh\left(\frac{z}{h}\right)$	$-\cosh\left(\frac{1}{2}\right)$
HTSDT [53]	$\frac{3\pi}{2}h\tanh\left(\frac{z}{h}\right)$	$-\frac{3\pi}{2}\mathrm{sech}^2\left(\frac{1}{2}\right)$
ESDT [30]	$ze^{-2(z/h)^2}$	0
SESDT [54]	$\sin\left(\frac{\pi z}{h}\right)e^{\frac{1}{2}\cos\left(\frac{\pi z}{h}\right)}$	$\frac{\pi}{2h}$
HSESDT [44]	$\sinh\left(\frac{z}{h}\right)e^{\frac{1}{5h}\cosh\left(\frac{z}{h}\right)}$	$-\frac{1}{h}[\cosh\left(\frac{1}{2}\right)+\frac{1}{5h}\sinh^2\left(\frac{1}{2}\right)]e^{\frac{1}{5h}\cosh\left(\frac{1}{2}\right)}$
HSPSDT [34]	$h\sinh\left(\frac{z}{h}\right)-\frac{4}{3}\frac{z^3}{h^2}\cosh\left(\frac{1}{2}\right)$	0
HTPSDT [35]	$\frac{h}{2}\tanh(2\frac{z}{h})-\frac{4}{3\cosh^2(1)}\left(\frac{z^3}{h^2}\right)$	0

The linear strain expressions derived from the displacement model of Eq. (23), valid for thin, moderately thick and thick plates, are:

$$\begin{Bmatrix} \varepsilon_x \\ \varepsilon_y \\ \gamma_{xy} \end{Bmatrix} = \begin{Bmatrix} \varepsilon_x^0 \\ \varepsilon_y^0 \\ \gamma_{xy}^0 \end{Bmatrix} + z\begin{Bmatrix} k_x^b \\ k_y^b \\ k_{xy}^b \end{Bmatrix} + f(z)\begin{Bmatrix} k_x^s \\ k_y^s \\ k_{xy}^s \end{Bmatrix},$$
$$\begin{Bmatrix} \gamma_{xz} \\ \gamma_{yz} \end{Bmatrix} = g(z)\begin{Bmatrix} \gamma_{xz}^0 \\ \gamma_{yz}^0 \end{Bmatrix}, \quad \varepsilon_z = g'(z)\varepsilon_z^0 \tag{26}$$

where

$$\begin{Bmatrix} \varepsilon_x^0 \\ \varepsilon_y^0 \\ \gamma_{xy}^0 \end{Bmatrix} = \begin{Bmatrix} \frac{\partial u_0}{\partial x} \\ \frac{\partial v_0}{\partial y} \\ \frac{\partial u_0}{\partial y} + \frac{\partial v_0}{\partial x} \end{Bmatrix}, \quad \begin{Bmatrix} k_x^b \\ k_y^b \\ k_{xy}^b \end{Bmatrix} = \begin{Bmatrix} -\frac{\partial^2 w_b}{\partial x^2} \\ -\frac{\partial^2 w_b}{\partial y^2} \\ -2\frac{\partial^2 w_b}{\partial x \partial y} \end{Bmatrix},$$
$$\begin{Bmatrix} k_x^s \\ k_y^s \\ k_{xy}^s \end{Bmatrix} = \begin{Bmatrix} -\frac{\partial^2 w_s}{\partial x^2} \\ -\frac{\partial^2 w_s}{\partial y^2} \\ -2\frac{\partial^2 w_s}{\partial x \partial y} \end{Bmatrix}, \quad \begin{Bmatrix} \gamma_{xz}^0 \\ \gamma_{yz}^0 \end{Bmatrix} = \begin{Bmatrix} \frac{\partial w_s}{\partial x} + \frac{\partial \varphi_z}{\partial x} \\ \frac{\partial w_s}{\partial y} + \frac{\partial \varphi_z}{\partial y} \end{Bmatrix}, \quad \varepsilon_z^0 = \varphi_z \tag{27}$$

2.3. Constitutive relations

The linear thermoelastic constitutive relations of orthotropic layers are given by:

$$\begin{Bmatrix} \sigma_1 \\ \sigma_2 \\ \sigma_3 \\ \tau_{12} \\ \tau_{13} \\ \tau_{23} \end{Bmatrix}^{(n)} = \begin{bmatrix} C_{11} & C_{12} & C_{13} & 0 & 0 & 0 \\ & C_{22} & C_{23} & 0 & 0 & 0 \\ & & C_{33} & 0 & 0 & 0 \\ & & & C_{44} & 0 & 0 \\ & \textbf{symmetric} & & & C_{55} & 0 \\ & & & & & C_{66} \end{bmatrix}^{(n)} \begin{Bmatrix} \varepsilon_1 - \alpha_1\Delta T \\ \varepsilon_2 - \alpha_2\Delta T \\ \varepsilon_3 - \alpha_3\Delta T \\ \gamma_{12} \\ \gamma_{13} \\ \gamma_{23} \end{Bmatrix}^{(n)} \tag{28}$$

By performing the transformation rule of stresses/strain between the lamina and the laminate coordinate system, the stress strain relations for the n-th lamina in the global coordinates (x, y, z) can be written as:

$$\begin{Bmatrix} \sigma_x \\ \sigma_y \\ \sigma_z \\ \tau_{xy} \\ \tau_{xz} \\ \tau_{yz} \end{Bmatrix}^{(n)} = \begin{bmatrix} Q_{11} & Q_{12} & Q_{13} & Q_{14} & 0 & 0 \\ & Q_{22} & Q_{23} & Q_{24} & 0 & 0 \\ & & Q_{33} & Q_{34} & 0 & 0 \\ & & & Q_{44} & 0 & 0 \\ & \textbf{symmetric} & & & Q_{55} & Q_{56} \\ & & & & & Q_{66} \end{bmatrix}^{(n)} \begin{Bmatrix} \varepsilon_x - \alpha_x\Delta T \\ \varepsilon_y - \alpha_y\Delta T \\ \varepsilon_z - \alpha_z\Delta T \\ \gamma_{xy} - \alpha_{xy}\Delta T \\ \gamma_{xz} \\ \gamma_{yz} \end{Bmatrix}^{(n)} \tag{29}$$

where ΔT is the temperature change from stress free state. While detailed expressions of the elements for matrices $[C]$ and $[Q]$ can be found in [55], the coefficients of thermal expansion for the n-th layer in the laminate reference coordinates are:

$$(\alpha_x, \alpha_y, \alpha_z, \alpha_{xy}, \alpha_{xz}, \alpha_{yz}) = (c^2\alpha_1 + s^2\alpha_2, s^2\alpha_1 + c^2\alpha_2, \alpha_3, 2sc(\alpha_1 - \alpha_2), 0, 0) \tag{30}$$

where $c = \cos\gamma$ and $s = \sin\gamma$, γ being the angle between the principal fiber direction x_1 and the x-axis of individual layers.

2.4. Initial thermal stresses

Under the thermal loading of uniform temperature variation ΔT, the prebuckling strains and stresses of a multi-layer plate can be given as:

$$\varepsilon_x = \varepsilon_y = \gamma_{xy} = \gamma_{yz} = \gamma_{xz} = 0, \text{ and } \sigma_{xz} = \sigma_{yz} = \sigma_z = 0 \tag{31}$$

Inserting Eq. (31) into the constitutive relations of Eq. (29), one obtains the nonzero prebuckling in-plane stresses (σ_x, σ_y, τ_{xy}) as:

$$\begin{Bmatrix} \sigma_x^0 \\ \sigma_y^0 \\ \tau_{xy}^0 \end{Bmatrix}^{(n)} = -\begin{Bmatrix} \left(Q_{11} - \frac{Q_{13}^2}{Q_{33}}\right)\alpha_x + \left(Q_{12} - \frac{Q_{13}Q_{23}}{Q_{33}}\right)\alpha_y + \left(Q_{14} - \frac{Q_{13}Q_{34}}{Q_{33}}\right)\alpha_{xy} \\ \left(Q_{12} - \frac{Q_{23}Q_{13}}{Q_{33}}\right)\alpha_x + \left(Q_{22} - \frac{Q_{23}^2}{Q_{33}}\right)\alpha_y + \left(Q_{24} - \frac{Q_{23}Q_{34}}{Q_{33}}\right)\alpha_{xy} \\ \left(Q_{14} - \frac{Q_{34}Q_{13}}{Q_{33}}\right)\alpha_x + \left(Q_{24} - \frac{Q_{34}Q_{23}}{Q_{33}}\right)\alpha_y + \left(Q_{44} - \frac{Q_{34}^2}{Q_{33}}\right)\alpha_{xy} \end{Bmatrix}^{(n)} \Delta T \tag{32}$$

The initial deformation induced by thermal loading is neglected in the present study.

2.5. Governing equations

Hamilton's principle is used to derive the governing equations of motion appropriate to the displacement field and the constitutive equation. The principle can be stated in analytical form as:

$$0 = \int_0^t (\delta U + \delta W - \delta T)\mathrm{d}t \tag{33}$$

The variation of strain energy U of the plate is calculated by:

$$\begin{aligned} \delta U &= \int_V \left(\sigma_x\delta\varepsilon_x + \sigma_y\delta\varepsilon_y + \sigma_z\delta\varepsilon_z + \tau_{xy}\delta\gamma_{xy} + \tau_{xz}\delta\gamma_{xz} + \tau_{yz}\delta\gamma_{yz}\right)\mathrm{d}V \\ &= \int_A \begin{pmatrix} N_x\delta\varepsilon_x^0 + N_y\delta\varepsilon_y^0 + N_z\delta\varepsilon_z^0 + N_{xy}\delta\gamma_{xy}^0 + S_{xz}^s\delta\gamma_{xz}^0 + S_{yz}^s\delta\gamma_{yz}^0 \\ + M_x^b\delta k_x^b + M_y^b\delta k_y^b + M_{xy}^b\delta k_{xy}^b + M_x^s\delta k_x^s + M_y^s\delta k_y^s + M_{xy}^s\delta k_{xy}^s \end{pmatrix}\mathrm{d}A \end{aligned} \tag{34}$$

where V is the whole volume of the sandwich plate and A is the top surface. (N_x, N_y, N_{xy}) denote the total in-plane force resultants, (M_x^b, M_y^b, M_{xy}^b) denote the total moment resultants, (M_x^s, M_y^s, M_{xy}^s) denote the additional stress couples associated with the transverse shear effects, N_z denote the transverse normal stress resultants, and (S_{xz}^s, S_{yz}^s) denote the transverse shear stress resultants, defined as:

$$\begin{aligned} &\begin{Bmatrix} N_x, & N_y, & N_{xy} \\ M_x^b, & M_y^b, & M_{xy}^b \\ M_x^s, & M_y^s, & M_{xy}^s \end{Bmatrix} = \sum_{n=1}^{K}\int_{h_{n-1}}^{h_n} (\sigma_x, \sigma_y, \tau_{xy})^{(n)} \begin{Bmatrix} 1 \\ z \\ f(z) \end{Bmatrix}\mathrm{d}z, \\ &N_z = \sum_{n=1}^{K}\int_{h_{n-1}}^{h_n} (\sigma_z)^{(n)} g'(z)\mathrm{d}z, \quad (S_{xz}^s, S_{yz}^s) = \sum_{n=1}^{K}\int_{h_{n-1}}^{h_n} (\tau_{xz}, \tau_{yz})^{(n)} g(z)\mathrm{d}z \end{aligned} \tag{35}$$

where K is the number of layers in the laminated composite or sandwich.

The variation of potential energy W of the in-plane loads induced by thermal stresses is:

$$\delta W = \int_V \begin{pmatrix} \sigma_x^0(u_{,x}\delta u_{,x} + v_{,x}\delta v_{,x} + w_{,x}\delta w_{,x}) \\ +\tau_{xy}^0\delta(u_{,x}u_{,y} + v_{,x}v_{,y} + w_{,x}w_{,y}) \\ +\sigma_x^0(u_{,y}\delta u_{,y} + v_{,y}\delta v_{,y} + w_{,y}\delta w_{,x}) \end{pmatrix}\mathrm{d}V \tag{36}$$

The variation of kinetic energy T of the plate is:

$$\begin{aligned} \delta T &= \int_V \rho(\dot{u}\delta\dot{u} + \dot{v}\delta\dot{v} + \dot{w}\delta\dot{w})\mathrm{d}V \\ &= \int_A \begin{Bmatrix} I_1\delta(\dot{u}_0^2 + \dot{v}_0^2 + \dot{w}_b^2 + \dot{w}_s^2 + 2\dot{w}_b\dot{w}_s) - 2I_2\delta(\dot{u}_0\dot{w}_{b,x} + \dot{v}_0\dot{w}_{b,y}) \\ +I_3\delta(\dot{w}_{b,x}^2 + \dot{w}_{b,y}^2) - 2I_4\delta(\dot{u}_0\dot{w}_{s,x} + \dot{v}_0\dot{w}_{s,y}) \\ +2I_5\delta(\dot{w}_{b,x}\dot{w}_{s,x} + \dot{w}_{b,y}\dot{w}_{s,y}) \\ +I_6\delta(\dot{w}_{s,x}^2 + \dot{w}_{s,y}^2) + 2I_7\delta(\dot{w}_b\dot{\varphi}_z + \dot{w}_s\dot{\varphi}_z) + I_8\delta\dot{\varphi}_z^2 \end{Bmatrix}\mathrm{d}x\mathrm{d}y \end{aligned} \tag{37}$$

where

$$(I_1, I_2, I_3, I_4, I_5, I_6, I_7, I_8) = \sum_{n=1}^{3}\int_{h_n}^{h_{n+1}} (1, z, z^2, f(z), zf(z), [f(z)]^2, g(z), [g(z)]^2)\rho(z)\mathrm{d}z \tag{38}$$

Upon substituting (34), (36) and (37) into (33) and integrating the resulting equation by parts and collecting the coefficients of δu_0, δv_0, δw_b, δw_s, and $\delta\varphi_z$, the equations of motion for the sandwich plate are obtained as:

$$\begin{aligned} &\delta u_0 : \frac{\partial N_x}{\partial x} + \frac{\partial N_{xy}}{\partial y} + \bar{N}_1 = I_1\ddot{u}_0 - I_2\ddot{w}_{b,x} - I_4\ddot{w}_{s,x} \\ &\delta v_0 : \frac{\partial N_{xy}}{\partial x} + \frac{\partial N_y}{\partial y} + \bar{N}_2 = I_1\ddot{v}_0 - I_2\ddot{w}_{b,y} - I_4\ddot{w}_{s,y} \\ &\delta w_b : \frac{\partial^2 M_x^b}{\partial x^2} + 2\frac{\partial^2 M_{xy}^b}{\partial x\partial y} + \frac{\partial^2 M_y^b}{\partial y^2} + +\bar{N}_3 = I_1(\ddot{w}_b + \ddot{w}_s)I_2(\ddot{u}_{0,x} + \ddot{v}_{0,y}) \\ &\quad - I_3(\ddot{w}_{b,xx} + \ddot{w}_{b,yy}) - I_5(\ddot{w}_{s,xx} + \ddot{w}_{s,yy}) + I_7\ddot{\varphi}_z \\ &\delta w_s : \frac{\partial^2 M_x^s}{\partial x^2} + 2\frac{\partial^2 M_{xy}^s}{\partial x\partial y} + \frac{\partial^2 M_y^s}{\partial y^2} + \frac{\partial S_{xz}^s}{\partial x} + \frac{\partial S_{yz}^s}{\partial y} \\ &\quad + \bar{N}_3 = I_1(\ddot{w}_b + \ddot{w}_s) + I_4(\ddot{u}_{0,x} + \ddot{v}_{0,y}) - I_5(\ddot{w}_{b,xx} + \ddot{w}_{b,yy}) \\ &\quad - I_6(\ddot{w}_{s,xx} + \ddot{w}_{s,yy}) + I_7\ddot{\varphi}_z\delta\varphi_z : \frac{\partial S_{xz}^s}{\partial x} + \frac{\partial S_{yz}^s}{\partial y} \\ &\quad - N_z + \bar{N}_4 = I_7(\ddot{w}_b + \ddot{w}_s) + I_8\ddot{\varphi}_z \end{aligned} \tag{39}$$

where the thermal loads $\bar{N}_i (i = 1, 2, 3, 4)$ are:

$$\begin{Bmatrix} \bar{N}_1 \\ \bar{N}_2 \\ \bar{N}_3 \\ \bar{N}_4 \end{Bmatrix} = \sum_{n=1}^{K}\int_{h_{n-1}}^{h_n} \left\{\sigma_x^0, \sigma_y^0, \tau_{xy}^0\right\}^{(n)} \begin{bmatrix} u_{,xx} & v_{,xx} & w_{,xx} & g(z)w_{,xx} \\ u_{,xy} & v_{,xy} & w_{,xy} & g(z)w_{,xy} \\ u_{,yy} & v_{,yy} & w_{,yy} & g(z)w_{,yy} \end{bmatrix}\mathrm{d}z \tag{40}$$

More detailed expressions of (40) are given in Appendix A.

By substituting Eq. (26) into Eq. (29) and the subsequent results into Eq. (35), the stress resultants are obtained as:

$$\begin{aligned} &\begin{Bmatrix} N \\ M^b \\ M^s \end{Bmatrix} = \begin{bmatrix} A & B & B^s \\ B & D & D^s \\ B^s & D^s & H^s \end{bmatrix}\begin{Bmatrix} \varepsilon \\ k^b \\ k^s \end{Bmatrix} + \begin{bmatrix} L \\ L^b \\ L^s \end{bmatrix}\varepsilon_z^0 - \begin{Bmatrix} N^T \\ M^{bT} \\ M^{sT} \end{Bmatrix}, S = A^s\gamma \\ &N_z = L^{\mathrm{T}}\varepsilon + (L^b)^{\mathrm{T}}k^b + (L^s)^{\mathrm{T}}k^s + R^s\varphi_z - N_z^T \end{aligned} \tag{41}$$

where

$$\begin{aligned} &N = \{N_x, N_y, N_{xy}\}^{\mathrm{T}}, \quad M^b = \{M_x^b, M_y^b, M_{xy}^b\}^{\mathrm{T}}, \\ &M^s = \{M_x^s, M_y^s, M_{xy}^s\}^{\mathrm{T}}\varepsilon = \{\varepsilon_x^0, \varepsilon_y^0, \varepsilon_{xy}^0\}^{\mathrm{T}}, \quad k^b = \{k_x^b, k_y^b, k_{xy}^b\}^{\mathrm{T}}, \\ &k^s = \{k_x^s, k_y^s, k_{xy}^s\}^{\mathrm{T}}N^T = \{N_x, N_y, N_{xy}\}^{\mathrm{T}}, \quad M^{bT} = \{M_x^{bT}, M_y^{bT}, M_{xy}^{bT}\}^{\mathrm{T}}, \\ &M^s = \{M_x^{sT}, M_y^{sT}, M_{xy}^{sT}\}^{\mathrm{T}}S = \{S_{xz}^s, S_{yz}^s\}^{\mathrm{T}}, \quad \gamma = \{\gamma_{xz}^0, \gamma_{yz}^0\}^{\mathrm{T}} \end{aligned} \tag{42}$$

$$A = \begin{bmatrix} A_{11} & A_{12} & A_{13} \\ A_{12} & A_{22} & A_{23} \\ A_{13} & A_{23} & A_{33} \end{bmatrix}, \quad B = \begin{bmatrix} B_{11} & B_{12} & B_{13} \\ B_{12} & B_{22} & B_{23} \\ B_{13} & B_{23} & B_{33} \end{bmatrix},$$
$$D = \begin{bmatrix} D_{11} & D_{12} & D_{13} \\ D_{12} & D_{22} & D_{23} \\ D_{13} & D_{23} & D_{33} \end{bmatrix} \tag{43}$$

$$B^s=\begin{bmatrix}B^s_{11} & B^s_{12} & B^s_{13}\\ B^s_{12} & B^s_{22} & B^s_{23}\\ B^s_{13} & B^s_{23} & B^s_{33}\end{bmatrix},\quad D^s=\begin{bmatrix}D^s_{11} & D^s_{12} & D^s_{13}\\ D^s_{12} & D^s_{22} & D^s_{23}\\ D^s_{13} & D^s_{23} & D^s_{33}\end{bmatrix},$$
$$H^s=\begin{bmatrix}H^s_{11} & H^s_{12} & H^s_{13}\\ H^s_{12} & H^s_{22} & H^s_{23}\\ H^s_{13} & H^s_{23} & H^s_{33}\end{bmatrix} \tag{44}$$

$$A^s=\begin{bmatrix}A^s_{11} & A^s_{12}\\ A^s_{12} & A^s_{22}\end{bmatrix},\quad L=\{L_1,L_2,L_3\}^{\mathrm{T}},\quad L^b=\{L^b_1,L^b_2,L^b_3\}^{\mathrm{T}},$$
$$L^s=\{L^s_1,L^s_2,L^s_3\}^{\mathrm{T}} \tag{45}$$

The stiffness coefficients A_{ij} and B_{ij}, ... are defined as:

$$\begin{Bmatrix}A_{11} & B_{11} & D_{11} & B^s_{11} & D^s_{11} & H^s_{11}\\ A_{12} & B_{12} & D_{12} & B^s_{12} & D^s_{12} & H^s_{12}\\ A_{13} & B_{13} & D_{13} & B^s_{13} & D^s_{13} & H^s_{13}\\ A_{22} & B_{22} & D_{22} & B^s_{22} & D^s_{22} & H^s_{22}\\ A_{23} & B_{23} & D_{23} & B^s_{23} & D^s_{23} & H^s_{23}\\ A_{33} & B_{33} & D_{33} & B^s_{33} & D^s_{33} & H^s_{33}\end{Bmatrix}$$
$$=\sum_{n=1}^{K}\int_{h_{n-1}}^{h_n}(1,z,z^2,f(z),zf(z),f^2(z))\begin{Bmatrix}Q_{11}\\ Q_{12}\\ Q_{14}\\ Q_{22}\\ Q_{24}\\ Q_{44}\end{Bmatrix}\mathrm{d}z \tag{46}$$

$$\begin{Bmatrix}L_1 & L^b_1 & L^s_1\\ L_2 & L^b_2 & L^s_2\\ L_3 & L^b_3 & L^s_3\end{Bmatrix}=\sum_{n=1}^{K}\int_{h_{n-1}}^{h_n}(1,z,f(z))g'(z)\begin{Bmatrix}Q_{13}\\ Q_{23}\\ Q_{34}\end{Bmatrix}\mathrm{d}z,$$
$$\begin{Bmatrix}A^s_{11}\\ A^s_{22}\\ A^s_{12}\end{Bmatrix}=\sum_{n=1}^{K}\int_{h_{n-1}}^{h_n}g^2(z)\begin{Bmatrix}Q_{55}\\ Q_{66}\\ Q_{56}\end{Bmatrix}\mathrm{d}z,R^s=\sum_{n=1}^{K}\int_{h_{n-1}}^{h_n}[g'(z)]^2Q_{33}\mathrm{d}z \tag{47}$$

The force and moment resultants $\{N^T\}$, N^T_z, $\{M^{bT}\}$ and $\{M^{sT}\}$ due to thermal loading are expressed as:

$$\begin{Bmatrix}N^T_x & M^{bT}_x & M^{sT}_x\\ N^T_y & M^{bT}_y & M^{sT}_y\\ N^T_{xy} & M^{bT}_{xy} & M^{sT}_{xy}\end{Bmatrix}=\sum_{n=1}^{K}\int_{h_{n-1}}^{h_n}(1,z,f(z))\begin{bmatrix}Q_{11} & Q_{12} & Q_{13} & Q_{14}\\ Q_{12} & Q_{22} & Q_{23} & Q_{24}\\ Q_{14} & Q_{24} & Q_{34} & Q_{44}\end{bmatrix}\begin{Bmatrix}\alpha_x\\ \alpha_y\\ \alpha_z\\ \alpha_{xy}\end{Bmatrix}\Delta T\mathrm{d}z$$
$$N^T_z=\sum_{n=1}^{K}\int_{h_{n-1}}^{h_n}\{Q_{13},Q_{23},Q_{33},Q_{34}\}g'(z)\{\alpha_x,\alpha_y,\alpha_z,\alpha_{xy}\}^T\Delta T\mathrm{d}z \tag{48}$$

It is worth mentioning that in thermal environment with uniform temperature change ΔT, N^T_z, $\{M^{bT}\}$ and $\{M^{sT}\}$ all vanish in the equations of motion expressed in terms of expanded displacement components.

Introducing Eqs. (42)(49) into (40), one can rewrite the equations of motion using the expanded displacement components (δu_0, δv_0, δw_b, δw_s, $\delta\varphi_z$), as:

$$(A_{11}d_{11}u_0+2A_{13}d_{12}u_0+A_{33}d_{22}u_0)+[A_{13}d_{11}v_0+(A_{12}+A_{33})d_{12}v_0+A_{23}d_{22}v_0]-[B_{11}d_{111}w_b+3B_{13}d_{112}w_b+(B_{12}+2B_{33})d_{122}w_b+B_{23}d_{222}w_b]-[B^s_{11}d_{111}w_s+3B^s_{13}d_{112}w_s+(B^s_{12}+2B^s_{33})d_{122}w_s+B^s_{23}d_{222}w_s]+(L_1d_1\varphi_z+L_3d_2\varphi_z)+\bar{N}_1=I_1\ddot{u}_0-I_2\ddot{w}_{b,x}-I_4\ddot{w}_{s,x} \tag{49}$$

$$(A_{33}d_{11}v_0+2A_{23}d_{12}v_0+A_{22}d_{22}v_0)+[A_{13}d_{11}u_0+(A_{12}+A_{33})d_{12}u_0+A_{23}d_{22}u_0]-[B_{13}d_{111}w_b+(B_{12}+2B_{33})d_{112}w_b+3B_{23}d_{122}w_b+B_{22}d_{222}w_b]-[B^s_{13}d_{111}w_s+(B^s_{12}+2B^s_{33})d_{112}w_s+3B^s_{23}d_{122}w_s+B^s_{22}d_{222}w_s]+(L_3d_1\varphi_z+L_2d_2\varphi_z)+\bar{N}_2=I_1\ddot{v}_0-I_2\ddot{w}_{b,y}-I_4\ddot{w}_{s,y} \tag{50}$$

$$[B_{11}d_{111}u_0+3B_{13}d_{112}u_0+(B_{12}+2B_{33})d_{122}u_0+B_{23}d_{222}u_0]+[B_{13}d_{111}v_0+(B_{12}+2B_{33})d_{112}v_0+3B_{23}d_{122}v_0+B_{22}d_{222}v_0]-[D_{11}d_{1111}w_b+4D_{13}d_{1112}w_b+(2D_{12}+4D_{33})d_{1122}w_b+4D_{23}d_{1222}w_b+D_{22}d_{2222}w_b]-[D^s_{11}d_{1111}w_s+4D^s_{13}d_{1112}w_s+(2D^s_{12}+4D^s_{33})d_{1122}w_s+4D^s_{23}d_{1222}w_s+D^s_{22}d_{2222}w_s]+(L^b_1d_{11}\varphi_z+2L^b_3d_{12}\varphi_z+L^b_2d_{22}\varphi_z)+\bar{N}_3=I_1(\ddot{w}_b+\ddot{w}_s)+I_2(\ddot{u}_{0,x}+\ddot{v}_{0,y})-I_3(\ddot{w}_{b,xx}+\ddot{w}_{b,yy})-I_5(\ddot{w}_{s,xx}+\ddot{w}_{s,yy})+I_7\ddot{\varphi}_z \tag{51}$$

$$[B^s_{11}d_{111}u_0+3B^s_{13}d_{112}u_0+(B^s_{12}+2B^s_{33})d_{122}u_0+B^s_{23}d_{222}u_0]+[B^s_{13}d_{111}v_0+(B^s_{12}+2B^s_{33})d_{112}v_0+3B^s_{23}d_{122}v_0+B^s_{22}d_{222}v_0]-[D^s_{11}d_{1111}w_b+4D^s_{13}d_{1112}w_b+(2D^s_{12}+4D^s_{33})d_{1122}w_b+4D^s_{23}d_{1222}w_b+D^s_{22}d_{2222}w_b]-[H^s_{11}d_{1111}w_s+4H^s_{13}d_{1112}w_s+(2H^s_{12}+4H^s_{33})d_{1122}w_s+4H^s_{23}d_{1222}w_s+H^s_{22}d_{2222}w_s]+(A^s_{11}d_{11}w_s+2A^s_{12}d_{12}w_s+A^s_{22}d_{22}w_s)+[(L^s_1+A^s_{11})d_{11}\varphi_z+(2L^s_3+2A^s_{12})d_{12}\varphi_z+(L^s_2+A^s_{22})d_{22}\varphi_z]+\bar{N}_3=I_1(\ddot{w}_b+\ddot{w}_s)+I_4(\ddot{u}_{0,x}+\ddot{v}_{0,y})-I_5(\ddot{w}_{b,xx}+\ddot{w}_{b,yy})-I_6(\ddot{w}_{s,xx}+\ddot{w}_{s,yy})+I_7\ddot{\varphi}_z \tag{52}$$

$$-(L_1d_1u_0+L_3d_2u_0)-(L_3d_1v_0+L_2d_2v_0)+(L^b_1d_{11}w_{b_b}+2L^b_3d_{12}w_b+L^b_2d_{22}w)+[(A^s_{11}+L^s_1)d_{11}w_s+(2L^s_3+2A^s_{12})d_{12}w_s+(A^s_{22}+L^s_2)d_{22}w_s]+(A^s_{11}d_{11}\varphi_z+2A^s_{12}d_{12}\varphi_z+A^s_{22}d_{22}\varphi_z-R^s\varphi_z)+\bar{N}_4=I_7(\ddot{w}_b+\ddot{w}_s)+I_8\ddot{\varphi}_z \tag{53}$$

where d_i, d_{ij}, d_{ijl} and d_{ijlm} are differential operators, defined by:

$$d_i=\frac{\partial}{\partial x_i},\quad d_{ij}=\frac{\partial^2}{\partial x_i\partial x_j},\quad d_{ijl}=\frac{\partial^3}{\partial x_i\partial x_j\partial x_l},\quad d_{ijlm}=\frac{\partial^4}{\partial x_i\partial x_j\partial x_l\partial x_m} \tag{54}$$

3. Solution procedure for eigenvalue problems

For illustration, the problem is solved under simply supported boundary conditions. The boundary conditions imposed at the side edges for shear deformation plate theories are:

$$\begin{aligned}&u_0(x,0)=w_b(x,0)=w_s(x,0)=\varphi_z(x,0)=0\\ &u_0(x,b)=w_b(x,b)=w_s(x,b)=\varphi_z(x,b)=0\\ &v_0(0,y)=w_b(0,y)=w_s(0,y)=\varphi_z(0,y)=0\\ &v_0(a,y)=w_b(a,y)=w_s(a,y)=\varphi_z(a,y)=0\\ &N_y(x,0)=M^b_y(x,0)=M^s_y(x,0)=N_y(x,b)=M^b_y(x,b)=M^s_y(x,b)=0\\ &N_x(0,y)=M^b_x(0,y)=M^s_x(0,y)=N_x(a,y)=M^b_x(a,y)=M^s_x(a,y)=0\end{aligned} \tag{55}$$

To obtain the structural responses of sandwich plate with cross-ply laminated plates, the displacement functions which satisfy the boundary conditions of (55) are selected as the following Fourier series:

$$\begin{Bmatrix}u_0\\ v_0\\ w_b\\ w_s\\ \varphi_z\end{Bmatrix}=\sum_{m=1}^{\infty}\sum_{n=1}^{\infty}\begin{Bmatrix}U_{mn}\cos(\lambda x)\sin(\mu y)\\ V_{mn}\sin(\lambda x)\cos(\mu y)\\ W_{bmn}\sin(\lambda x)\sin(\mu y)\\ W_{smn}\sin(\lambda x)\sin(\mu y)\\ Z_{mn}\sin(\lambda x)\sin(\mu y)\end{Bmatrix}e^{i\omega t} \tag{56}$$

Table 2
Material properties used for numerical validation against literature results.

Material 1
E_1/E_2 =open, $E_3 = E_2$, $G_{12} = G_{13} = 0.6E_2$, $G_{23} = 0.5E_2$, $\upsilon_{12} = \upsilon_{13} = \upsilon_{23} = 0.25$
Material 2
Face sheets
$E_1 = 131$GPa, $E_2 = 10.34$ GPa, $E_3 = E_2$, $G_{12} = 6.895$ GPa, $G_{13} = 6.205$ GPa, $G_{23} = 6.895$ GPa, $\upsilon_{12} = 0.22$, $\upsilon_{13} = 0.22$, $\upsilon_{23} = 0.49$, $\rho = 1627$ kg/m^3
Core
$E_1 = E_2 = E_3 = 6.89 \times 10^{-3}$GPa, $G_{12} = G_{13} = G_{23} = 3.45 \times 10^{-3}$ GPa, $\upsilon_{12} = \upsilon_{13} = \upsilon_{23} = 0$, $\rho = 97$ kg/m^3
Material 3
Face sheets
$E_1/E_2 = 19$,$E_3 = E_2$, $G_{12}/E_2 = 0.52$, $G_{13} = G_{12}$, $G_{23}/E_2 = 0.338$, $\upsilon_{12} = 0.32$, $\upsilon_{13} = \upsilon_{12}$, $\upsilon_{23} = 0.49$, $\alpha_1/\alpha_2 = 0.001$, $\alpha_3 = \alpha_2$
Core
$E_1/E_2^f = 3.2 \times 10^{-5}$,$E_2/E_2^f = 2.9 \times 10^{-5}$, $E_3/E_2^f = 0.4$, $G_{12}/E_2^f = 2.4 \times 10^{-3}$, $G_{13}/E_2^f = 7.9 \times 10^{-2}$, $G_{23}/E_2^f = 6.6 \times 10^{-2}$, $\upsilon_{12} = 0.99$, $\upsilon_{13} = \upsilon_{23} = 3.0 \times 10^{-5}$, $\alpha_1/\alpha_2^f = 1.36$, $\alpha_3 = \alpha_2 = \alpha_1$

Table 4
Comparison of non-dimensional natural frequencies $= \omega a^2/h\sqrt{\rho/E_2}$ $(\Delta T = 0)$ of simply supported cross-ply laminated square plates with $E_1/E_2 = 40$ (Material 1).*

Lamination andnumber of layers	Theory	a/h			
		10	20	50	100
$[0^\circ/90^\circ]$	A	10.4319	11.0663	11.2688	11.2988
	B	10.5680	11.1052	11.2751	11.3002
	C	10.5680	11.1052	11.2751	11.3002
	PSDT3	10.5023	11.0967	11.2715	11.3005
	TSDT	10.502	11.0965	11.2715	11.3004
	HSSDT	10.5012	11.0963	11.2714	11.3004
	HTPSDT	10.5262	11.0964	11.2707	11.2997
	HSPSDT	10.5025	11.0967	11.2715	11.3003
$[0^\circ/90^\circ/90^\circ/0^\circ]$	A	15.1048	17.6470	18.6720	18.8357
	B	15.1073	17.6457	18.6718	18.8356
	C	15.9405	17.9938	18.7381	18.8526
	PSDT3	15.1203	17.6975	18.7088	18.8358
	TSDT	15.1202	17.6975	18.7088	18.8358
	HSSDT	15.1202	17.6975	18.7088	18.8358
	HTPSDT	15.1251	17.7026	18.7113	18.835
	HSPSDT	15.1203	17.6975	18.7088	18.8357

* A: Results from Kant and Swaminathan [58] with 12 unknown variables; B: Results from Reddy [27]; C: Results from Senthilnathan et al. [59].

Table 3
Comparison of non-dimensional natural frequencies$= \omega a^2/h\sqrt{\rho/E_2}$ $(\Delta T = 0)$ of simply supported cross-ply laminated square plates with $a/h = 5$ (Material 1).*

Lamination andnumber of layers	Theory	E_1/E_2				
		3	10	20	30	40
$[0^\circ/90^\circ]$	A	6.2578	6.9845	7.6745	8.1763	8.5625
	PSDT3	6.2340 (−0.38)	7.0026 (0.26)	7.8326 (2.06)	8.5150 (4.14)	9.0959 (6.23)
	TSDT	6.2339 (−0.38)	7.0023 (0.25)	7.8322 (2.05)	8.5143 (4.13)	9.0948 (6.22)
	HSSDT	6.2337 (−0.39)	7.0018 (0.25)	7.8311 (2.04)	8.5127 (4.11)	9.0927 (6.19)
	HTPSDT[a]	6.2448 (−0.21)	7.0204 (0.51)	7.8631 (2.46)	8.5592 (4.68)	9.1544 (6.91)
	HSPSDT[a]	6.2340 (−0.38)	7.0027 (0.26) $[0^\circ/90^\circ]_2$	7.8328 (2.06)	8.5153 (4.15)	9.0963 (6.23)
	HTPSDT[b]	6.3734 (1.85)	7.1056 (1.73)	7.9279 (3.30)	8.6119 (5.33)	9.1986 (7.43)
	HSPSDT[b]	6.3698 (1.79)	7.0931 (1.55)	7.9016 (2.96)	8.5711 (4.83)	9.1428 (6.78)
$[0^\circ/90^\circ]_2$	A	6.5455	8.1445	9.4055	10.1650	10.6798
	PSDT3	6.5200 (−0.39)	8.2156 (0.87)	9.6456 (2.55)	10.5520 (3.81)	11.1867 (4.75)
	TSDT	6.5199 (−0.39)	8.2157 (0.87)	9.6458 (2.55)	10.5520 (3.81)	11.1871 (4.75)
	HSSDT	6.5199 (−0.39)	8.2159 (0.88)	9.6462 (2.56)	10.5529 (3.82)	11.1878 (4.76)
	HTPSDT[a]	6.5275 (−0.27)	8.2172 (0.89)	9.6412 (2.51)	10.5440 (3.73)	11.1771 (4.66)
	HSPSDT[a]	6.5199 (−0.39)	8.2157 (0.87)	9.6456 (2.55)	10.5518 (3.81)	11.1866 (4.75)
	HTPSDT[b]	6.6509 (1.61)	8.2715 (1.56)	9.6653 (2.76)	10.5560 (3.85)	11.1833 (4.71)
	HSPSDT[b]	6.6496 (1.59)	8.2742 (1.59)	9.6728 (2.84)	10.5661 (3.95)	11.1945 (4.82)
$[0^\circ/90^\circ]_3$	A	6.61	8.4143	9.8398	10.6958	11.2728
	PSDT3	6.5749 (−0.53)	8.4250 (0.13)	9.9363 (0.98)	10.8707 (1.64)	11.5150 (2.15)
	TSDT	6.5748 (−0.53)	8.4249 (0.13)	9.9362 (0.98)	10.8706 (1.63)	11.5149 (2.15)
	HSSDT	6.5747 (−0.53)	8.4249 (0.13)	9.9362 (0.98)	10.8705 (1.63)	11.5146 (2.14)
	HTPSDT[a]	6.5836 (−0.4)	8.4330 (0.22)	9.9464 (1.08)	10.8849 (1.77)	11.5345 (2.32)
	HSPSDT[a]	6.5749 (−0.53)	8.4250 (0.13)	9.9363 (0.98)	10.8707 (1.64)	11.5151 (2.15)
	HTPSDT[b]	6.7062 (1.46)	8.4847 (0.84)	9.9684 (1.31)	10.8953 (1.87)	11.5397 (2.37)
	HSPSDT[b]	6.7040 (1.42)	8.4810 (0.79)	9.9616 (1.24)	10.8833 (1.75)	11.5218 (2.21)
$[0^\circ/90^\circ]_5$	A	6.6458	8.5625	10.0843	11.0027	11.6245
	PSDT3	6.6033 (−0.64)	8.5321 (−0.36)	10.0850 (0.007)	11.0349 (0.29)	11.6861 (0.53)
	TSDT	6.6032 (−0.64)	8.5320 (−0.36)	10.0848 (0.005)	11.0347 (0.29)	11.6858 (0.53)
	HSSDT	6.6031 (−0.64)	8.5318 (−0.36)	10.0846 (0.003)	11.0343 (0.29)	11.6851 (0.52)
	HTPSDT[a]	6.6125 (−0.5)	8.5424 (−0.23)	10.1002 (0.16)	11.0568 (0.49)	11.7056 (0.7)
	HSPSDT[a]	6.6033 (−0.64)	8.5321 (−0.36)	10.0850 (0.007)	11.0350 (0.29)	11.6862 (0.53)
	HTPSDT[b]	6.7348 (1.33)	8.5930 (0.36)	10.1213 (0.37)	11.0668 (0.58)	11.7205 (0.83)
	HSPSDT[b]	6.7323 (1.30)	8.5870 (0.29)	10.1090 (0.24)	11.0470 (0.40)	11.6926 (0.59)
$[0^\circ/90^\circ/90^\circ/0^\circ]$	A	6.6815	8.2103	9.563	10.272	10.752
	PSDT3	6.6494 (−0.48)	8.3223 (1.36)	9.8488 (3.02)	10.6980 (4.15)	11.3036 (5.13)
	TSDT	6.6493 (−0.48)	8.3222 (1.36)	9.8486 (3.02)	10.6977 (4.14)	11.3032 (5.13)
	HSSDT	6.6492 (−0.48)	8.3220 (1.36)	9.8482 (3.01)	10.6971 (4.14)	11.3023 (5.12)
	HTPSDT[a]	6.6588 (−0.34)	8.3336 (1.50)	9.8663 (3.20)	10.7233 (4.39)	11.3376 (5.45)
	HSPSDT[a]	6.6494 (−0.48)	8.3224 (1.37)	9.8489 (3.02)	10.6981 (4.15)	11.3038 (5.13)
	HTPSDT[b]	6.7510 (1.04)	8.6537 (5.40)	10.2070 (6.76)	11.1631 (8.68)	11.8224 (9.96)
	HSPSDT[b]	6.7483 (1.00)	8.6468 (5.31)	10.1924 (6.61)	11.1398 (8.45)	11.7900 (9.66)

* A: 3D elasticity solution [56]. Superscripts a and b denote the cases of including and neglecting the effect of thickness stretching for HTPSDT and HSPSDT, respectively. For PSDT3, TSDT, and HSSDT, the effect of thickness stretching is included. Numbers in parentheses are percentage errors relative to 3D elasticity solutions.

Table 5
Comparison of non-dimensional natural frequencies $= \omega a^2/h\sqrt{(\rho/E_2)_f}(\Delta T = 0)$ of 5-layer antisymmetric sandwich square plates $[0^\circ/90^\circ/Core/0^\circ/90^\circ]$ with $h_c/h_f = 10$ (Material 2).*

Theory	a/h			
	10	20	50	100
A	4.8594	8.5955	13.6899	15.5093
B	7.0473	11.2664	15.0323	15.9522
C	7.0473	11.2664	15.0323	15.5522
PSDT3	5.0032	8.9424	13.7946	15.5333
TSDT	5.0242	8.9455	13.8023	15.5356
HSSDT	5.0479	8.9891	13.8183	15.5403
HTPSDT	4.9720	8.9196	13.7851	15.5191
HSPSDT	4.9194	8.9162	13.8005	15.5324

* A: Results from Kant and Swaminathan [58] with 12 unknown variables; B: Results from Reddy [27]; C: Results from Senthilnathan et al. [59].

where $i = \sqrt{-1}$, $\lambda = m\pi/a$, $\mu = n\pi/b$, and $(U_{mn}, V_{mn}, W_{bmn}, W_{smn}, Z_{mn})$ are arbitrary parameters (to be determined) and ω is the eigenfrequency associated with the (m, n)th eigenmode. Upon substituting (56) into (49)(53), the dynamic equation can be expressed as the following eigenvalue problem:

$$([\mathbf{K}] - \Delta T[\mathbf{K}_G] - \omega^2[\mathbf{M}])\{\Delta\} = \{\mathbf{0}\} \tag{57}$$

where $[\mathbf{K}]$ is the structural stiffness matrix, $[\mathbf{K}_G]$ is the geometric stiffness matrix induced by initial in-plane thermal stresses, $[\mathbf{M}]$ denotes the mass matrix, and $\{\Delta\}^T = \{U_{mn}, V_{mn}, W_{bmn}, W_{smn}, Z_{mn}\}$, for which the expressions are all presented in Appendix B. For stability analysis, Eq. (57) is reduced to:

$$([\mathbf{K}] - \Delta T[\mathbf{K}_G])\{\Delta\} = \{\mathbf{0}\} \tag{58}$$

For the present study, although all the eigenvalues and eigenvectors can be computed using the above method for each deformation mode of m and n, the dominant eigenvalues corresponding to the lowest natural frequencies and minimum critical temperature variations are of particular concern.

For CPT, SFDT and other higher-order theories without considering thickness stretching effect, the solution procedures are similar to those outlined above but are associated with less unknown variables and hence are not shown here.

4. Numerical results and discussions

4.1. Validation studies

4.1.1. Comparison with literature results

In Tables 3–6, the natural frequencies and critical temperature changes predicted by the present theories are compared with existing results, with relevant material properties employed in this subsection listed in Table 2. Tables 3 and 4 present dimensionless natural frequencies of simply supported multilayered cross-ply laminated composite square plates for selected modulus ratios (E_1/E_2) and side-to-thickness ratios (a/h). Tables 5 and 6 present dimensionless natural frequencies and critical temperature changes of simply supported sandwich square plates with multilayered cross-ply laminated face sheets.

The results of Tables 3–6 demonstrate that, for all the parameters considered, the frequency values and critical temperature changes predicted by the present RSTs (i.e., PSDT3, TSDT, HSSDT, HTPSDT, and HSPSDT) are in good agreement with those obtained using 3D elasticity solutions [56,57] and other higher order shear theories [58,59]. Nonetheless, the present RST models somewhat overestimate the fundamental frequencies and critical

Table 6
Comparison of non-dimensional critical temperature change $\underline{\Delta T} = \Delta T\alpha_2^f$ for symmetric sandwich square plates with 10-layer cross-ply laminated face sheets ($[0^\circ/90^\circ]_5$[**Core**]$[90^\circ/0^\circ]_5$, Material 3).*

a/h	Theory	h_f/h				
		0.025	0.05	0.075	0.1	0.15
10	A	0.3220	0.2737	0.2358	0.2072	0.1632
	PSDT3	0.3379 (4.94)	0.2862(4.57)	0.2445 (3.69)	0.2144 (3.47)	0.1709 (4.72)
	TSDT	0.3379 (4.94)	0.2861 (4.53)	0.2445 (3.69)	0.2144 (3.47)	0.1709 (4.72)
	HSSDT	0.3377 (4.88)	0.2860 (4.50)	0.2444 (3.65)	0.2144 (3.47)	0.1710 (4.78)
	HTPSDT	0.3384 (5.09)	0.2889 (5.55)	0.2474 (4.92)	0.2158 (4.15)	0.1691 (3.61)
	HSPSDT	0.3381 (5.00)	0.2862 (4.57)	0.2445 (3.69)	0.2144 (3.47)	0.1709 (4.72)
20	A	0.0929	0.0855	0.0791	0.0726	0.0623
	PSDT3	0.0971 (4.52)	0.0887 (3.74)	0.0812 (2.62)	0.0748 (3.03)	0.0651 (4.49)
	TSDT	0.0971 (4.52)	0.0887 (3.74)	0.0812 (2.65)	0.0748 (3.03)	0.0651 (4.49)
	HSSDT	0.0970 (4.41)	0.0886 (3.63)	0.0812 (2.62)	0.0748 (3.03)	0.0651 (4.49)
	HTPSDT	0.0977 (5.17)	0.0895 (4.68)	0.0819 (3.54)	0.0753 (3.72)	0.0650 (4.33)
	HSPSDT	0.0971 (4.52)	0.0887 (3.74)	0.0812 (2.62)	0.0748 (3.03)	0.0651 (4.49)

* A: 3D elasticity solutions [57]. Numbers in parentheses are percentage errors relative to 3D elasticity solutions.

Table 7
Mechanical properties of (a) foam and (b) base material of face sheets and corrugated panel.*

Material	Density	Young's modulus	Shear modulus	Poisson ratio	Thermal expansion coefficient
(a) Foam	ρ_f (g/cm^3)	E_f (MPa)	——	ν_f	α^f (10^{-6}/K)
Rohacell 31 (R31)	0.031	36	——	0.2	37
Rohacell 51 (R51)	0.052	70	——	0.3	33
Rohacell 71 (R71)	0.075	105	——	0.25	30
Alporas (aluminum)	0.230	1000	——	0.15	22
(b) Base material	ρ_s (g/cm^3)	E_s (GPa)	G_s (GPa)	ν	α_s (10^{-6}/K)
304 stainless steel	7.9	210	——	0.3	12
Ti-6Al-4V	4.43	114	——	0.33	8.6
T700/3234 composite	1.55	$E_1 = 110$, $E_2 = 8.7$, $E_3 = E_2$	$G_{12} = 4$, $G_{13} = G_{12}$ $G_{23} = 4$,	$\upsilon_{12} = 0.32$, $\upsilon_{13} = \upsilon_{12}$ $\upsilon_{23} = 0.3$	$\alpha_1 = 0.42$, $\alpha_2 = 28$, $\alpha_3 = \alpha_2$

Table 8
Comparison of dimensionless natural frequencies $\bar{\omega} = 100\omega a\sqrt{(\rho/E_1)_l}$ and critical temperature changes $\overline{\Delta T_{cr}} = \Delta T_{cr}\alpha_2^l \times 10^3$ of R31 foam-filled composite corrugated sandwich plates with 4-layer cross-ply laminated face sheets ($[0^\circ/90^\circ]_2$[**Core**][$90^\circ/0^\circ]_2$; for the corrugated core, $t/l = 0.05$, $b/a = 1$, $\theta = 45^\circ$, $h_f/h = 0.10$, and corrugation fiber is perpendicular to the prismatic direction).

a/h	Methods	$\bar{\omega}$ with $\Delta T = 0$	$\overline{\Delta T_{cr}}$
24	FEM	17.984	29.955
	HTPSDT	17.146	28.510
	HSPSDT	17.146	28.525
48	FEM	9.025	7.544
	HTPSDT	8.683	7.300
	HSPSDT	8.687	7.306
72	FEM	5.862	3.323
	HTPSDT	5.803	3.259
	HSPSDT	5.805	3.262

temperature changes, since the assumed displacement field cannot account for significant change of materials properties between adjacent layers. Table 3 shows that the prediction error associated with the present RSTs relative to 3D elasticity solutions increases with increasing E_1/E_2 and decreases with the increase in layer number. Results obtained from the present RST models with effect of thickness stretching taken into account are more or less the same. The natural frequencies of cross-ply laminated composite plates obtained by neglecting thickness stretching are slightly overestimated in comparison with those calculated with thickness stretching included, which is similar to the case of functionally graded plates [60]. Moreover, the HSPSDT appears to yield better predictions than HTPSDT. Unless otherwise stated, RST models with thickness stretching included are employed in subsequent discussions.

4.1.2. Finite element validation

It should be noted that at present there exists no study, either theoretical or experimental, on the vibration and buckling behaviors of foam-filled composite corrugated sandwich plates.

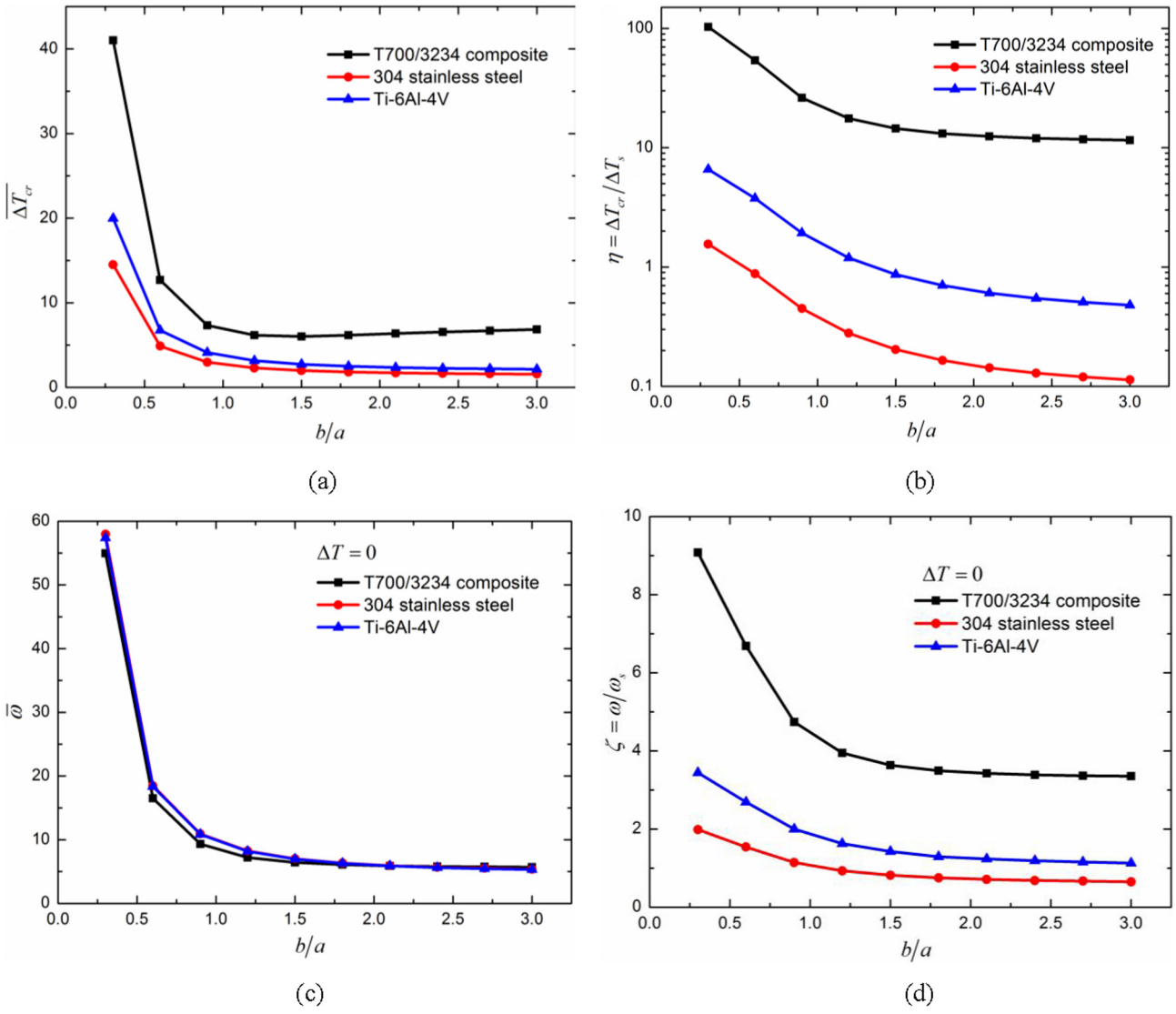

Fig. 4. Effect of aspect ratio b/a on (a) critical temperature change $\overline{\Delta T_{cr}}$, (b) nondimensional critical temperature change η, (c) natural frequency $\bar{\omega}$, and (d) nondimensional natural frequency ζ, for R31 foam-filled corrugated sandwich plates with face sheets and corrugation made of different materials ($t/l = 0.05, b/a = 1, \theta = 45^\circ$, and $h_f/h = 0.10$). The T700/3224 composite corrugated sandwich ($[0^\circ/90^\circ]_2$[Core][$90^\circ/0^\circ]_2$) is made of 4-layer cross-ply laminated face sheets and unidirectional laminated corrugation with fiber perpendicular to the prismatic direction.

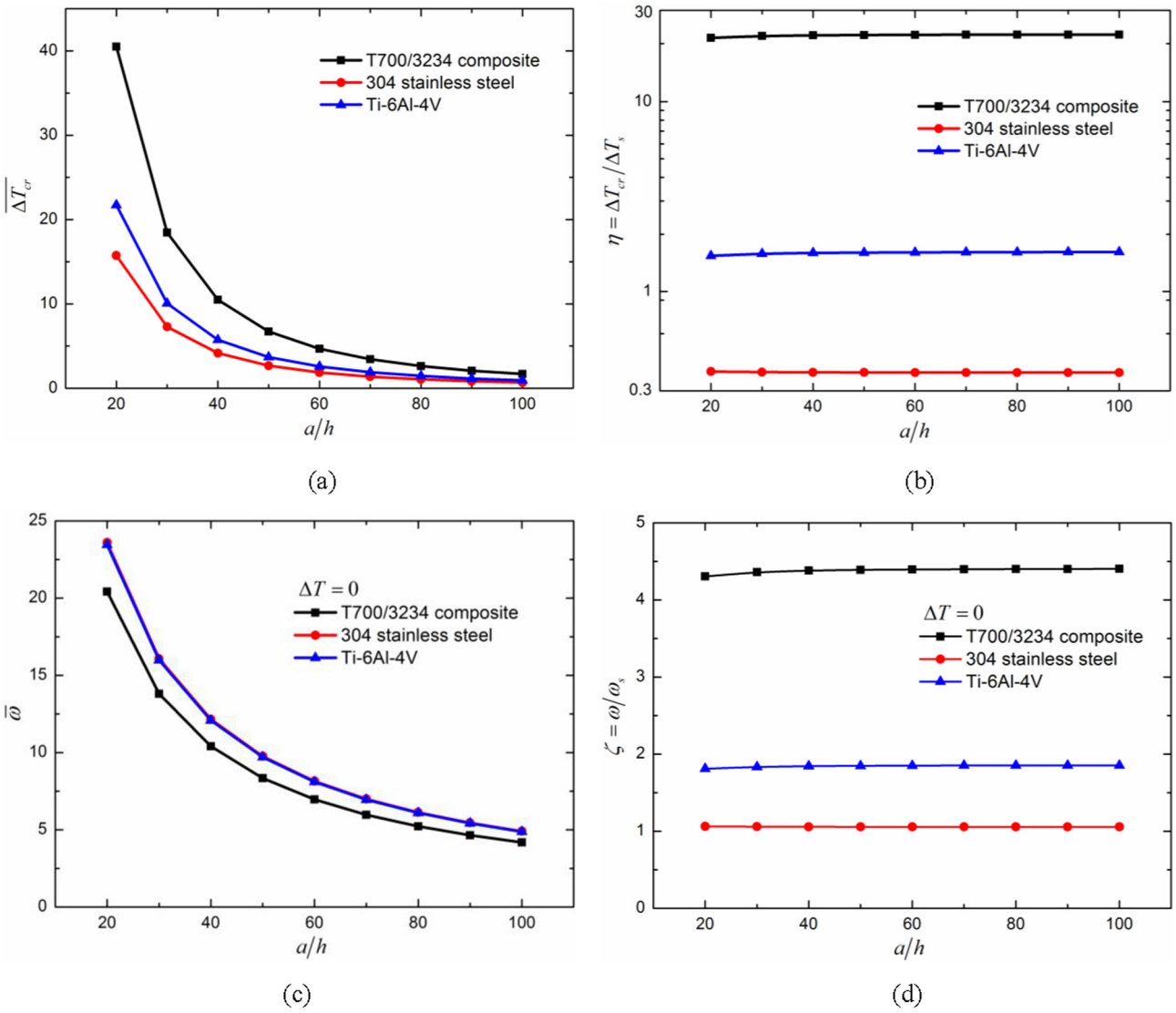

Fig. 5. Effect of side-to-thickness ratio a/h on (a) critical temperature change $\overline{\Delta T_{cr}}$, (b) nondimensional critical temperature change η, (c) natural frequency $\bar{\omega}$, and (d) nondimensional natural frequency ζ, for R31 foam-filled corrugated sandwich plates with face sheets and corrugation made of different materials ($t/l = 0.05, a/h = 50, \theta = 45^\circ$, and $h_f/h = 0.10$). The T700/3224 composite corrugated sandwich ($[0^\circ/90^\circ]_2$[**Core**]$[90^\circ/0^\circ]_2$) is made of 4-layer cross-ply laminated face sheets and unidirectional laminated corrugation with fiber perpendicular to the prismatic direction.

Therefore, to validate the current analysis, finite element (FE) simulations via commercially available FE code ABAQUS are carried out. A 20-node brick element with parabolic basis function C3D20R, which yields more accurate stresses than shell elements in the thickness direction, is used to model the foam filler and face sheets. Corrugated core members are modeled using an 8-node second-order shell element S8R5 with reduced integration. The embedded element technique is invoked to simulate the mutual effect between foam matrix and corrugated members, where the shell elements of corrugated panels (i.e. S8R5 as the embedded elements) are embedded in the solid elements of foam core (i.e. C3D20R as the host elements). Perfect bonding is assumed at the interfaces between the core and face sheets. Simply supported boundary conditions are implemented using coupling constraints. A linear perturbation analysis step is applied to extract the natural frequency and critical buckling temperature change. For symmetric polymer foam Rohacell 31-filled T700/3234 composite corrugated sandwich square plates (Table 7), the face sheets are made of 4-layer cross-ply laminates, the corrugated members are made of unidirectional laminates (with fiber perpendicular to the prismatic direction of core), and the side-to-thickness ratio a/h is varied from 24 to 72, with $t/l = 0.05$, $\theta = 45^\circ$ and $h_f/h = 0.10$.

As is shown in Table 8, good agreement between FEM simulation results and theoretical predictions obtained from both the HTPSDT and HSPSDT models is achieved. (Extra FEM simulations have been carried out for the validation study, as shown in latter Figs. 7 and 10.) The effectiveness of combining the homogenization technique and the refined shear deformation plate theory is thus demonstrated for foam-filled corrugated sandwich structures. Typically, the theoretical predictions are slightly smaller than the FEM results, since errors in calculating the overall properties of the equivalent continuum are inevitable. In the following section, the HSPSDT model is employed to investigate systematically the performance of foam-filled corrugated sandwich plates.

4.2. Parametric study of critical temperature change and natural frequency

The effects of geometric and material parameters on the thermal stability and free vibration of symmetric foam-filled

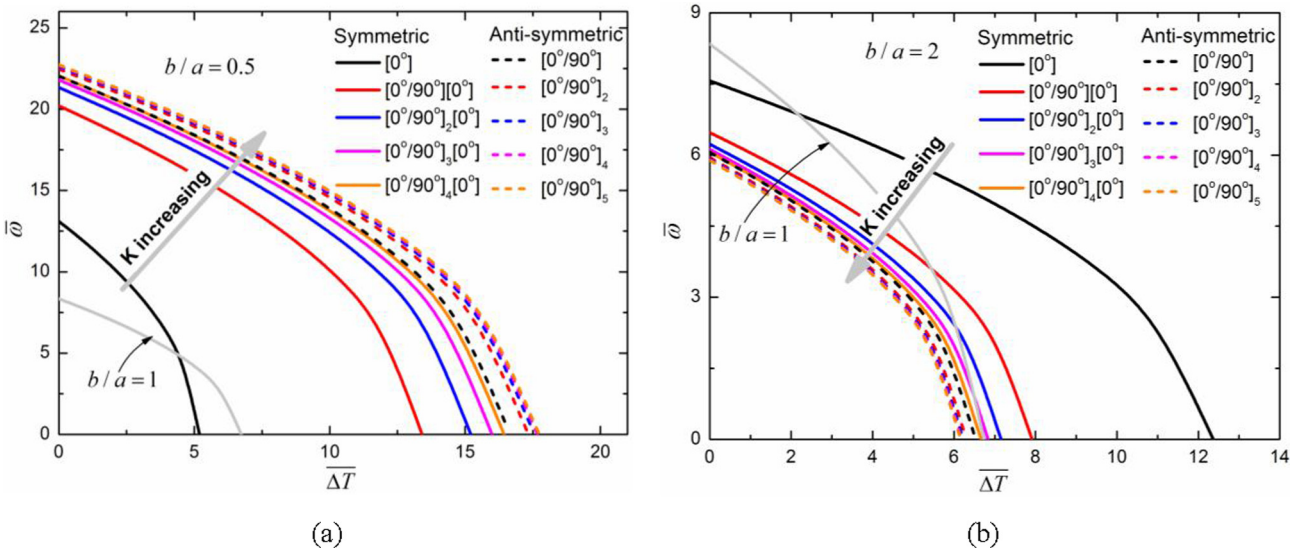

Fig. 6. Effect of layer number of cross-ply laminated face sheets on dimensionless natural frequency and critical temperature change, with the stacking sequence classified into symmetric type ($[0°/90°]_K[0°]$) and *anti*-symmetric type ($[0°/90°]_K$): (a) $b/a = 0.5$ and (b) $b/a = 2$. Parameter K (ranging from 0 to 5) denotes layer number of face sheets.

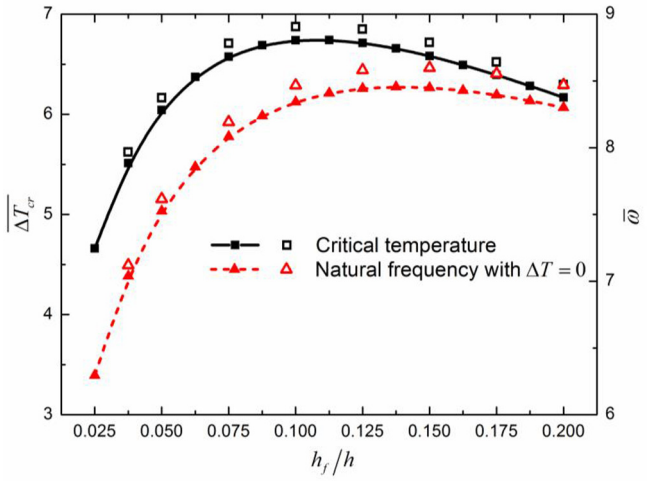

Fig. 7. Effect of face-to-thickness ratio h_f/h on critical temperature change and natural frequency of symmetric T700/3234 laminated composite corrugated sandwich plate having $b/a = 1$, $a/h = 50$, $t/l = 0.05$ and $\theta = 45°$. Solid symbols refer to the theoretical predictions while hollow symbols denote the results from FEM.

corrugated sandwich plates are quantified. For convenience, dimensionless natural frequency and critical buckling temperature change are introduced, as:

$$\bar{\omega} = 100\omega a\sqrt{(\rho/E_1)_l}, \quad \overline{\Delta T}_{cr} = \Delta T_{cr}\alpha_2^l \times 10^3 \tag{59}$$

where the superscript/subscript l denotes laminated composite (T700/3234). Further, to reveal the superiority of foam-filled corrugated sandwich plates over more conventional solid structures, two nondimensional parameters are defined as:

$$\eta = \Delta T_{cr}/\Delta T_s, \quad \zeta = \omega/\omega_s \tag{60}$$

where ΔT_s and ω_s are the critical temperature change and natural frequency of a T700/3234 unidirectional laminated composite (fiber along the x-direction) solid plate having the same weight, length, width and boundary conditions as those of the present sandwich plate. Then the thickness of the reference solid plate is:

$$h_s = (2h_f\rho_s + h_c\rho_c)/\rho_l \tag{61}$$

4.2.1. Effects of aspect ratio and side-to-thickness ratio

Figs. 4 and 5 show the effects of aspect ratio b/a and side-to-thickness ratio a/h on the critical temperature change and natural frequency of R31 foam-filled corrugated sandwich plates with face sheets and corrugation made of different materials: T700/3234 graphite/epoxy laminated composite, 304 stainless steel, and Ti-6Al-4V (Table 7). It is worth mentioning that the composite corrugated sandwich plate is made of cross-ply laminated face sheets and unidirectional laminated corrugated panels.

As can be observed from Figs. 4a, c and 5 5a, c, the critical temperature change and natural frequency decrease rapidly with increasing b/a or a/h. The results of Figs. 4b, d and 5b, d demonstrate that the T700/3234 composite corrugated sandwich plate exhibits the highest structural efficiency due to the highest stiffness-to-mass ratio of its parent material. In contrast, the sandwich plate made of 304 stainless steel is even inferior to the T700/3234 composite solid plate, *i.e.*, the reference plate. Moreover, the non-dimensional critical temperature η and frequency ζ decrease as b/a increases, but almost remain constant as a/h increases. This implies that the structural efficiency of a foam-filled corrugated sandwich plate decreases by increasing b/a, but remains almost the same as a/h is varied.

Subsequent discussions are all limited to symmetric T700/3234 laminated composite corrugated sandwich plates having $b/a = 1$ and $a/h = 50$.

4.2.2. Effects of layer number and face-to-thickness ratio of cross-ply laminated composite face sheets

Influence of layer number of cross-ply laminated composite face sheets upon the natural frequency (plotted as a function of temperature change) is presented in Fig. 6, for representative values of the aspect ratio b/a. The stacking sequence of the face sheets is classified into symmetric type $[0°/90°]_K[0°]$ and anti-symmetric type $[0°/90°]_K$, where K denotes the layer number of face sheets. It is seen from Fig. 6 that the natural frequency decreases monotonically to zero when the temperature change is increased to the critical buckling one, because the stiffness of the matrix $([\mathbf{K}] - \Delta T[\mathbf{K}_G])$ decreases rapidly as soon as the temperature change reaches the critical one. It is also intriguing to find that square sandwich plates ($b/a = 1$) are insensitive to variations of K. In contrast, for rectangular plates with $b/a = 0.5$ (Fig. 6a), the critical

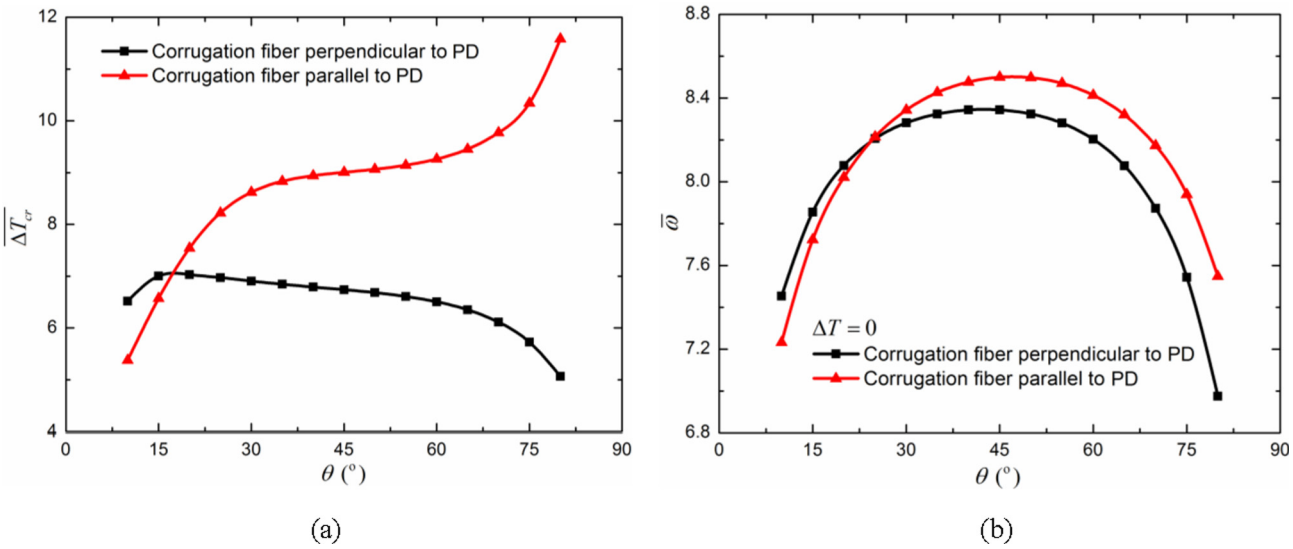

Fig. 8. Effects of corrugation angle and fiber stacking direction of corrugation on (a) critical temperature change and (b) natural frequency of symmetric T700/3234 laminated composite corrugated sandwich plate having $b/a = 1$, $a/h = 50$, $h_f/h = 0.10$, and $t/l = 0.05$.

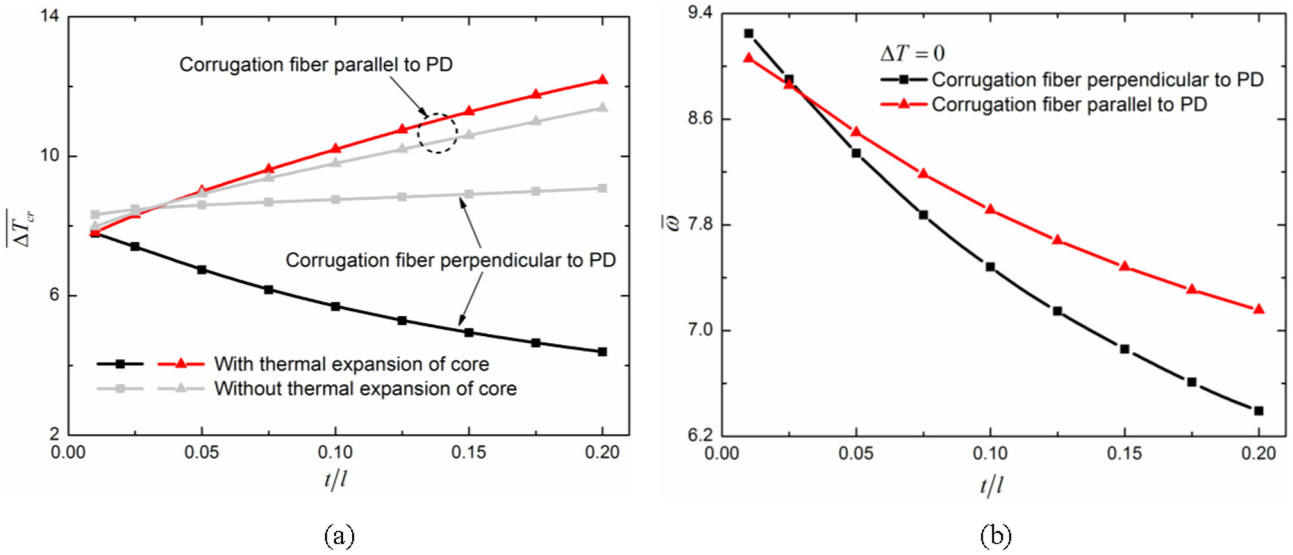

Fig. 9. Effects of corrugation slenderness and fiber stacking direction of corrugation on (a) critical temperature change and (b) natural frequency of symmetric T700/3234 laminated composite corrugated sandwich plate having $b/a = 1$, $a/h = 50$, $h_f/h = 0.10$, and $\theta = 45°$. In Fig. 9a, the results obtained by neglecting the thermal expansion of foam-filled corrugated core are included as reference.

temperature change and natural frequency increase as K is increased. In general, sandwich plates with anti-symmetric face sheets are superior to those with symmetric face sheets; however, the tendency is reversed for plates with $b/a = 2$ (Fig. 6b).

The dependence of critical temperature change and natural frequency upon face-to-thickness ratio h_f/h is presented in Fig. 7. Both initially increase and then gradually decrease as h_f/h is increased. The value of h_f/h for maximal critical temperature change is different from that causing maximal natural frequency.

4.2.3. Effects of geometric parameters and fiber stacking orientation of corrugation

The effects of corrugation angle and corrugation slenderness on critical temperature change and natural frequency are shown in Figs. 8 and 9, respectively. Two cases of unidirectional corrugation fiber perpendicular and parallel to the prismatic direction (PD) are considered, defined as Case A and Case B, respectively. It is seen from Fig. 8a that the critical temperature change increases monotonically with increasing θ for Case B, but increases first and then decreases with increasing θ for Case A. In contrast, the natural frequency increases first and then decreases with θ, peaking at $\theta = 45°$ for both cases (Fig. 8b). As shown in Fig. 9a, as the corrugation slenderness increases from 0.01 to 0.2, the critical temperature change increases for Case B and decreases for Case A. For comparison, the results obtained by neglecting the thermal expansion of foam-filled corrugated core are also presented as gray lines in Fig. 9a. The large deviation of the gray lines from the solid lines indicates the significant influence of sandwich core thermal expansion on critical temperature change. Moreover, with the increase of corrugation slenderness, the density of the core increases, resulting in higher structural weight but smaller natural frequency (Fig. 9b). The results of Figs. 8 and 9 also imply that the critical temperature change and natural frequency for Case B are generally larger than those for Case A.

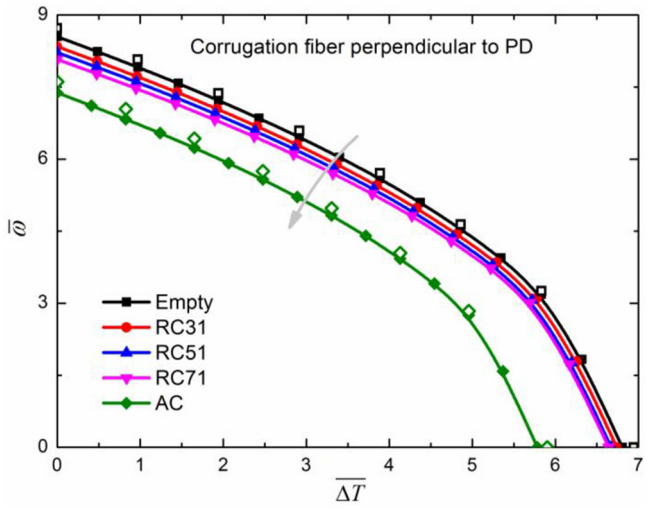

Fig. 10. Effects of foam material on natural frequency as a function of temperature change for the symmetric T700/3234 laminated composite corrugated sandwich plate ($b/a = 1$, $a/h = 50$, $h_f/h = 0.10$, $t/l = 0.05$ and $\theta = 45°$) having the corrugation fiber perpendicular to prismatic direction (PD). Solid symbols refer to the theoretical predictions while hollow symbols denotes the results from FEM. For brevity, only the FE calculated results of sandwich plates with empty and Alporas foam-filled corrugated cores are added in the figure.

4.2.4. Effect of foam material

To explore the influence of foam filler, Fig. 10 plots the natural frequency as a function of temperature change for the foam materials listed in Table 7. Let RC31, RC51, RC71 and AC denote composite corrugated sandwich plates filled with Rohacell 31 (R31), Rohacell 51 (R51), Rohacell 71 (R71), and aluminum foam (Alporas), respectively, and let Empty denote un-filled corrugated sandwiches. It is striking to find that foam filling slightly reduces the natural frequency and critical temperature change of corrugated sandwich plates by 2.4–13.7%. A stiffer foam leads to smaller natural frequency and critical temperature change, because the foam filling contributes little to the structural stiffness but increases the structural weight and thermal expansion coefficient. However, the tendency may be reversed, or at least the difference between sandwiches with and without foam-filling may be smaller in higher frequencies due to the occurrence of local vibration modes. Extra FE simulations (not shown here for brevity) reveal that foam filling can effectively suppress local buckling and local vibration.

5. Conclusions

Free vibration and buckling of foam-filled composite corrugated sandwich plates under uniform thermal loading are investigated theoretically. The refined shear and normal deformation theory incorporating two kinds of combinations of hyperbolic and parabolic shear shape functions is employed, with the foam-filled corrugated core treated as homogeneous continuum with equivalent material properties. The main conclusions are summarized as follows:

1) The present theoretical predictions are in good agreement with the results from literature and FE simulations, validating the effectiveness of the refined shear deformation theory with combined hyperbolic and parabolic shape functions and the thermo-elastic homogenization procedure of foam-filled composite corrugated sandwich cores.
2) The combined hyperbolic-sin and polynomial shear deformation theory predicts better than the combined hyperbolic-tangent and polynomial shear deformation theory.
3) T700/3234 composite corrugated sandwich plates have the highest structural efficiency due to the highest stiffness-to-mass ratio of the carbon fiber-reinforced composite, compared with those made of Ti-6Al-4V and 304 stainless steel.
4) Aspects including the aspect ratio, side-to-thickness ratio, layer number and face-to-thickness ratio of cross-ply laminated face sheets, together with the geometric parameters and fiber stacking orientation of unidirectional composite corrugation affect significantly the natural frequency and critical temperature change of foam-filled composite corrugated sandwich plates. Corrugation fiber parallel to the prismatic direction with corrugation angle of $\theta = 45°$ leads to the highest natural frequency and moderately higher critical temperature change.
5) Foam filling slightly decreases the global natural frequency and critical temperature change of corrugated sandwich plates by 2.4%~13.7%.
6) The present study provides an efficient approach of vibration and stability analysis for foam-filled composite sandwich plates subjected to mechanical and thermal loadings, and can be extended to cover other types of sandwich or multilayer plate s.

Acknowledgments

This work was supported by the National Natural Science Foundation of China (11472209, 51375369 and 11472208), China Postdoctoral Science Foundation (2016M600782), Postdoctoral Scientific Research Project of Shaanxi Province (2016BSHYDZZ18) and the Fundamental Research Funds for Xi'an Jiaotong University (xjj2015102).

Appendix A. Detailed expressions of the thermal loads

By substituting Eq. (23) into Eq. (40), the thermal loads $\bar{N}_i (i = 1, 2, 3, 4)$ are obtained as:

$$\begin{Bmatrix} \bar{N}_1 \\ \bar{N}_2 \\ \bar{N}_3 \\ \bar{N}_4 \end{Bmatrix} = \begin{Bmatrix} A_x^{T1} d_{11} u_0 + 2A_{xy}^{T1} d_{12} u_0 + A_y^{T1} d_{22} u_0 + A_x^{T2} d_{111} w_b + 2A_{xy}^{T2} d_{112} w_b + A_y^{T2} d_{122} w_b + A_x^{T3} d_{111} w_s + 2A_{xy}^{T3} d_{112} w_s + A_y^{T3} d_{122} w_s \\ A_x^{T1} d_{11} v_0 + 2A_{xy}^{T1} d_{12} v_0 + A_y^{T1} d_{22} v_0 + A_x^{T2} d_{112} w_b + 2A_{xy}^{T2} d_{122} w_b + A_y^{T2} d_{222} w_b + A_x^{T3} d_{112} w_s + 2A_{xy}^{T3} d_{122} w_s + A_y^{T3} d_{222} w_s \\ A_x^{T1} d_{11} w_b + 2A_{xy}^{T1} d_{12} w_b + A_y^{T1} d_{22} w_b + A_x^{T1} d_{11} w_s + 2A_{xy}^{T1} d_{12} w_s + A_y^{T1} d_{22} w_s + A_x^{T4} d_{11} \varphi_z + 2A_{xy}^{T4} d_{12} \varphi_z + A_y^{T4} d_{22} \varphi_z \\ A_x^{T4} d_{11} w_b + 2A_{xy}^{T4} d_{12} w_b + A_y^{T4} d_{22} w_b + A_x^{T4} d_{11} w_s + 2A_{xy}^{T4} d_{12} w_s + A_y^{T4} d_{22} w_s + A_x^{T5} d_{11} \varphi_z + 2A_{xy}^{T5} d_{12} \varphi_z + A_y^{T5} d_{22} \varphi_z \end{Bmatrix} \quad (A.1)$$

where

$$\begin{Bmatrix} A_x^{Ti} \\ A_{xy}^{Ti} \\ A_y^{Ti} \end{Bmatrix} = \sum_{n=1}^{K} \int_{h_{n-1}}^{h_n} F_i(z) \begin{Bmatrix} (Q_{11} - \frac{Q_{13}^2}{Q_{33}})\alpha_x + (Q_{12} - \frac{Q_{13}Q_{23}}{Q_{33}})\alpha_y + (Q_{14} - \frac{Q_{13}Q_{34}}{Q_{33}})\alpha_{xy} \\ (Q_{12} - \frac{Q_{23}Q_{13}}{Q_{33}})\alpha_x + (Q_{22} - \frac{Q_{23}^2}{Q_{33}})\alpha_y + (Q_{24} - \frac{Q_{23}Q_{34}}{Q_{33}})\alpha_{xy} \\ (Q_{14} - \frac{Q_{34}Q_{13}}{Q_{33}})\alpha_x + (Q_{24} - \frac{Q_{34}Q_{23}}{Q_{33}})\alpha_y + (Q_{44} - \frac{Q_{34}^2}{Q_{33}})\alpha_{xy} \end{Bmatrix}^{(n)} dz, \quad (i = 1, 2, \ldots, 5) \tag{A.2}$$

The functions $F_i(z)$ (i=1,2, ..,5) are expressed by:

$$\{F_1(z), F_2(z), F_3(z), F_4(z), \quad F_5(z)\} = \{1, z, f(z), g(z), g^2(z)\} \tag{A.3}$$

Appendix B. Elements of [K], [K_G] and [M] matrices

The structural stiffness matrix is:

$$[\mathbf{K}] = \begin{bmatrix} k_{1,1} & k_{1,2} & k_{1,3} & k_{1,4} & k_{1,5} \\ & k_{2,2} & k_{2,3} & k_{2,4} & k_{2,5} \\ & & k_{3,3} & k_{3,4} & k_{3,5} \\ & \textbf{symmetric} & & k_{4,4} & k_{4,5} \\ & & & & k_{5,5} \end{bmatrix} \tag{B.1}$$

where

$$\begin{aligned}
&k_{1,1} = A_{11}\lambda^2 + A_{33}\mu^2, k_{1,2} = (A_{12} + A_{33})\lambda\mu, \\
&k_{1,3} = -[B_{11}\lambda^2 + (B_{12} + 2B_{33})\mu^2]\lambda, \\
&k_{1,4} = -[B_{11}^s\lambda^2 + (B_{12}^s + 2B_{33}^s)\mu^2]\lambda, k_{1,5} = -L_1\lambda, \\
&k_{2,2} = A_{33}\lambda^2 + A_{22}\mu^2, k_{2,3} = -[(B_{12} + 2B_{33})\lambda^2 + B_{22}\mu^2]\mu, \\
&k_{2,4} = -[(B_{12}^s + 2B_{33}^s)\lambda^2 + B_{22}^s\mu^2]\mu, \quad k_{2,5} = -L_2\mu, \\
&k_{3,3} = D_{11}\lambda^4 + (2D_{12} + 4D_{33})\lambda^2\mu^2 + D_{22}\mu^4, \\
&k_{3,4} = D_{11}^s\lambda^4 + (2D_{12}^s + 4D_{33}^s)\lambda^2\mu^2 + D_{22}^s\mu^4, \\
&k_{3,5} = L_1^b\lambda^2 + L_2^b\mu^2, \\
&k_{4,4} = H_{11}^s\lambda^4 + (2H_{12}^s + 4H_{33}^s)\lambda^2\mu^2 + H_{22}^s\mu^4 + A_{11}^s\lambda^2 + A_{22}^s\mu^2, \\
&k_{4,5} = (L_1^s + A_{11}^s)\lambda^2 + (L_2^s + A_{22}^s)\mu^2, \\
&k_{5,5} = A_{11}^s\lambda^2 + A_{22}^s\mu^2 + R^s
\end{aligned} \tag{B.2}$$

The geometric stiffness matrix induced by initial in-plane thermal stresses is:

$$[\mathbf{K}_G] = \begin{bmatrix} k_{1,1}^g & k_{1,2}^g & k_{1,3}^g & k_{1,4}^g & k_{1,5}^g \\ k_{2,1}^g & k_{2,2}^g & k_{2,3}^g & k_{2,4}^g & k_{2,5}^g \\ k_{3,1}^g & k_{3,2}^g & k_{3,3}^g & k_{3,4}^g & k_{3,5}^g \\ k_{4,1}^g & k_{4,2}^g & k_{4,3}^g & k_{4,4}^g & k_{4,5}^g \\ k_{5,1}^g & k_{5,2}^g & k_{5,3}^g & k_{5,4}^g & k_{5,5}^g \end{bmatrix} \tag{B.3}$$

where

$$\begin{aligned}
&k_{1,1}^g = A_x^{T1}\lambda^2 + A_y^{T1}\mu^2, k_{1,2}^g = 0, k_{1,3}^g = -(A_x^{T2}\lambda^2 + A_y^{T2}\mu^2)\lambda, \\
&k_{1,4}^g = -(A_x^{T3}\lambda^2 + A_y^{T3}\mu^2)\lambda, k_{1,5}^g = 0 k_{2,1}^g = 0, \\
&k_{2,2}^g = k_{1,1}^g, k_{2,3}^g = -(A_x^{T2}\lambda^2 + A_y^{T2}\mu^2)\mu, k_{2,4}^g = -(A_x^{T3}\lambda^2 + A_y^{T3}\mu^2)\mu, \\
&k_{2,5}^g = 0 k_{3,1}^g = 0, k_{3,2}^g = 0, k_{3,3}^g = k_{1,1}^g, k_{3,4}^g = k_{1,1}^g, \\
&k_{3,5}^g = A_x^{T4}\lambda^2 + A_y^{T4}\mu^2, k_{4,i}^g = k_{3,i}^g, (i = 1, 2, \ldots, 5) k_{5,1}^g = 0, k_{5,2}^g = 0, \\
&k_{5,3}^g = k_{3,5}^g, k_{5,4}^g = k_{4,5}^g, k_{5,5}^g = A_x^{T5}\lambda^2 + A_y^{T5}\mu^2
\end{aligned} \tag{B.4}$$

The mass matrix is:

$$[\mathbf{M}] = \begin{bmatrix} m_{1,1} & m_{1,2} & m_{1,3} & m_{1,4} & m_{1,5} \\ & m_{2,2} & m_{2,3} & m_{2,4} & m_{2,5} \\ & & m_{3,3} & m_{3,4} & m_{3,5} \\ & \textbf{symmetric} & & m_{4,4} & m_{4,5} \\ & & & & m_{5,5} \end{bmatrix} \tag{B.5}$$

where

$$\begin{aligned}
&m_{1,1} = I_1, m_{1,2} = 0, \quad m_{1,3} = -I_2\lambda, \quad m_{1,4} = -I_4\lambda, \quad m_{1,5} = 0, \\
&m_{2,2} = m_{1,1}, \quad m_{2,3} = -I_2\mu, \quad m_{2,4} = -I_4\mu, \quad m_{2,5} = 0, \\
&m_{3,3} = I_1 + I_3(\lambda^2 + \mu^2), \quad m_{3,4} = I_1 + I_5(\lambda^2 + \mu^2), \quad m_{3,5} = I_7, \\
&m_{4,4} = I_1 + I_6(\lambda^2 + \mu^2), \quad m_{4,5} = m_{3,5}, \\
&m_{5,5} = I_8
\end{aligned} \tag{B.6}$$

References

[1] Evans AG, Hutchinson JW, Fleck NA, Ashby MF, Wadley HNG. The topological design of multifunctional cellular metals. Prog Mater Sci 2001;46(3–4):309–27.
[2] Wadley HNG. Multifunctional periodic cellular metals. Philos Trans R Soc A 1838;2006(364):31–68.
[3] Torrez JB. Light-weight materials selection for high-speed naval craft. Massachusetts Inst Tech Cambridge 2007.
[4] Cote F, Deshpande VS, Fleck NA, Evans AG. The compressive and shear responses of corrugated and diamond lattice materials. Int J Solids Struct 2006;43(20):6220–42.
[5] Valdevit L, Hutchinson JW, Evans AG. Structurally optimized sandwich panels with prismatic cores. Int J Solids Struct 2004;41(18–19):5105–24.
[6] Valdevit L, Wei Z, Mercer C, Zok FW, Evans AG. Structural performance of near-optimal sandwich panels with corrugated cores. Int J Solids Struct 2006;43(16):4888–905.
[7] Vaziri A, Xue Z, Hutchinson JW. Metal sandwich plates with polymer foam-filled cores. J Mech Mater Struct 2006;1(1):97–127.
[8] Yan LL, Yu B, Han B, Chen CQ, Zhang QC, Lu TJ. Compressive strength and energy absorption of sandwich panels with aluminum foam-filled corrugated cores. Compos Sci Technol 2013;86:142–8.
[9] Han B, Yan LL, Yu B, Zhang QC, Chen CQ, Lu TJ. Collapse mechanisms of metallic sandwich structures with aluminum foam-filled corrugated cores. J Mech Mater Struct 2014;9(4):397–425.
[10] Yu B, Han B, Ni CY, Zhang QC, Chen CQ, Lu TJ. Dynamic crushing of all-metallic corrugated panels filled with close-celled aluminum foams. ASME J Appl Mech 2015;82(1).
[11] Yan LL, Han B, Yu B, Chen CQ, Zhang QC, Lu TJ. Three-point bending of sandwich beams with aluminum foam-filled corrugated cores. Mater Des 2014;60:510–9.
[12] Han B, Wen C, Yu B, Ni CY, Qin KK, Zhang QC. Collapse mechanism analysis of foam-filled corrugated sandwich beams under in-plane compression. J Xi'an Jiaotong Univ 2014;48(11):37–43.
[13] Han B, Yu B, Xu Y, Chen CQ, Zhang QC, Lu TJ. Foam filling radically enhances transverse shear response of corrugated sandwich plates. Mater Des 2015;77:132–41.
[14] Han B, Qin KK, Yu B, Zhang QC, Chen CQ, Lu TJ. Design optimization of foam-reinforced corrugated sandwich beams. Compos Struct 2015;130:51–62.
[15] Han B, Zhang ZJ, Zhang QC, Zhang Q, Lu TJ, Lu BH. Recent advances in hybrid lattice-cored sandwiches for enhanced multifunctional performance. Extreme Mech Lett 2017;10:58–69.
[16] Han B. Mechanical behaviors of reinforced corrugated composite cellular materials (Ph.D. Dissertation). Xi'an Jiaotong University; 2015.
[17] Lou J, Ma L, Wu LZ. Free vibration analysis of simply supported sandwich beams with lattice truss core. Mater Sci Eng B-Adv 2012;177(19):1712–6.
[18] Lou J, Wang B, Ma L, Wu LZ. Free vibration analysis of lattice sandwich beams under several typical boundary conditions. Acta Mech Solida Sin 2013;26(5):458–67.
[19] Xu MH, Qiu ZP. Free vibration analysis and optimization of composite lattice truss core sandwich beams with interval parameters. Compos Struct 2013;106:85–95.
[20] Sayyad AS, Ghugal YM. On the free vibration analysis of laminated composite and sandwich plates: a review of recent literature with some numerical results. Compos Struct 2015;129:177–201.
[21] Carrera E, Brischetto S. A survey with numerical assessment of classical and refined theories for the analysis of sandwich plates. Appl Mech Rev 2009;62:1–17.
[22] Kreja I. A literature review on computational models for laminated composite and sandwich panels. Open Eng 2011;1(1):59–80.

[23] Swaminathan K, Naveenkumar DT, Zenkour AM, Carrera E. Stress, vibration and buckling analyses of FGM plates—A state-of-the-art review. Compos Struct 2015;120:10–31.
[24] Birman V, Byrd LW. Modeling and analysis of functionally graded materials and structures. Appl Mech Rev 2007;60(5):195–216.
[25] Jha DK, Kant T, Singh RK. A critical review of recent research on functionally graded plates. Compos Struct 2013;96:833–49.
[26] Thai HT, Kim SE. A review of theories for the modeling and analysis of functionally graded plates and shells. Compos Struct 2015;128:70–86.
[27] Reddy JN. A simple higher-order theory for laminated composite plates. J Appl Mech 1984;51(4):745–52.
[28] Touratier M. An efficient standard plate theory. Int J Eng Sci 1991;29 (8):901–16.
[29] Mantari JL, Oktem AS, Soares CG. A new trigonometric shear deformation theory for isotropic, laminated composite and sandwich plates. Int J Solids Struct 2012;49(1):43–53.
[30] Karama M, Afaq KS, Mistou S. Mechanical behavior of laminated composite beam by new multi-layered laminated composite structures model with transverse shear stress continuity. Int J Solids Struct 2003;40(6):1525–46.
[31] Aydogdu M. A new shear deformation theory for laminated composite plates. Compos Struct 2009;89(1):94–101.
[32] Soldatos KP. A transverse-shear deformation-theory for homogeneous monoclinic plates. Acta Mech 1992;94(3–4):195–220.
[33] Ghugal YM, Pawar MD. Buckling and vibration of plates by hyperbolic shear deformation theory. J Aerosp Eng Technol 2011;1(1):1–12.
[34] Zenkour AM. A simple four-unknown refined theory for bending analysis of functionally graded plates. Appl Math Model 2013;37(20–21):9041–51.
[35] Amale M, El Abbas AB, Tounsi A. A new hyperbolic shear deformation theory for bending and free vibration analysis of isotropic, functionally graded, sandwich and laminated composite plates. Appl Math Model 2015;39: 2489–508.
[36] Grover N, Singh BN, Maiti DK. Analytical and finite element modeling of laminated composite and sandwich plates: an assessment of a new shear deformation theory for free vibration response. Int J Mech Sci 2013;67:89–99.
[37] Aydogdu M. Comparison of various shear deformation theories for bending, buckling, and vibration of rectangular symmetric cross-ply plate with simply supported edges. J Compos Mater 2006;40(23):2143–55.
[38] Thai H-T, Choi D-H. Improved refined plate theory accounting for effect of thickness stretching in functionally graded plates. Compos Part B-Eng 2014;56:705–16.
[39] Shimpi RP. Refined plate theory and its variants. AIAA J 2002;40(1):137–46.
[40] Houari MSA, Tounsi A, Beg OA. Thermoelastic bending analysis of functionally graded sandwich plates using a new higher order shear and normal deformation theory. Int J Mech Sci 2013;76:102–11.
[41] Hadji L, Atmane HA, Tounsi A, Mechab I, Bedia EAA. Free vibration of functionally graded sandwich plates using four-variable refined plate theory. Appl Math Mech-Engl 2011;32(7):925–42.
[42] Thai HT, Vo TP. A new sinusoidal shear deformation theory for bending, buckling, and vibration of functionally graded plates. Appl Math Model 2013;37(5):3269–81.
[43] Thai HT, Choi DH. Efficient higher-order shear deformation theories for bending and free vibration analyses of functionally graded plates. Arch Appl Mech 2013;83(12):1755–71.
[44] Belabed Z, Houari MSA, Tounsi A, Mahmoud SR, Beg OA. An efficient and simple higher order shear and normal deformation theory for functionally graded material (FGM) plates. Compos Part B-Eng 2014;60:274–83.
[45] Faure N, Doyoyo M. Thermomechanical properties of strut-lattices. J Mech Phys Solids 2007;55(4):803–18.
[46] Lu TJ, Liu T, Deng ZC. Thermoelastic properties of sandwich materials with pin-reinforced foam cores. Sci China Ser E 2008;51(12):2059–74.
[47] Thai HT, Kim SE. A simple quasi-3D sinusoidal shear deformation theory for functionally graded plates. Compos Struct 2013;99:172–80.
[48] Bessaim A, Houari MSA, Tounsi A, Mahmoud SR, Bedia EA. A new higher-order shear and normal deformation theory for the static and free vibration analysis of sandwich plates with functionally graded isotropic face sheets. J Sandw Struct Mater 2013;15(6):671–703.
[49] Lee WH, Han SC, Park WT. A refined higher order shear and normal deformation theory for E-, P-, and S-FGM plates on Pasternak elastic foundation. Compos Struct 2015;122:330–42.
[50] Thai HT, Choi DH. A simple first-order shear deformation theory for the bending and free vibration analysis of functionally graded plates. Compos Struct 2013;101:332–40.
[51] Ambartsumian SA. On theory of bending plates. Isz Otd Tech Nauk AN SSSR 1958;5:69–77.
[52] Reissner E. On transverse bending of plates, including the effect of transverse shear deformation. Int J Solids Struct 1975;11:569–73.
[53] Akavci SS. Two new hyperbolic shear displacement models for orthotropic laminated composite plates. Mech Compos Mater 2010;46(2):215–26.
[54] Mantari JL, Oktem AS, Soares CG. A new higher order shear deformation theory for sandwich and composite laminated plates. Compos Part B-Eng 2012;43 (3):1489–99.
[55] Matsunaga H. Free vibration and stability of angle-ply laminated composite and sandwich plates under thermal loading. Compos Struct 2007;77 (2):249–62.
[56] Noor AK. Free vibrations of multilayered composite plates. AIAA J 1973;11 (7):1038–9.
[57] Noor AK, Burton WS. Three-dimensional solutions for thermal buckling of multilayered anisotropic plates. J Eng Mech 1992;118(5):683–701.
[58] Kant T, Swaminathan K. Analytical solutions for free vibration of laminated composite and sandwich plates based on a higher-order refined theory. Compos Struct 2001;53(1):73–85.
[59] Senthilnathan NR, Lim SP, Lee KH, Chow ST. Buckling of shear-deformable plates. AIAA J 1987;25(9):1268–71.
[60] Alijani F, Amabili M. Effect of thickness deformation on large-amplitude vibrations of functionally graded rectangular plates. Compos Struct 2014;113:89–107.